Journal of
Mechanics of Materials and Structures

PIEZOELECTRIC SHELL THEORIES WITH *A PRIORI* CONTINUOUS TRANSVERSE ELECTROMECHANICAL VARIABLES

Erasmo Carrera and Salvatore Brischetto

Volume 2, Nº 2 *February 2007*

mathematical sciences publishers

JOURNAL OF MECHANICS OF MATERIALS AND STRUCTURES
Vol. 2, No. 2, 2007

PIEZOELECTRIC SHELL THEORIES WITH *A PRIORI* CONTINUOUS TRANSVERSE ELECTROMECHANICAL VARIABLES

ERASMO CARRERA AND SALVATORE BRISCHETTO

This paper addresses the static analysis of multilayer shells with embedded piezoelectric materials. The Reissner Mixed Variational Theorem is used to obtain transverse electromechanical variables (transverse shear and normal stresses, plus normal electrical displacement) which are *a priori* continuous at each layer-interface. The governing differential equations of doubly curved shells are derived by referring to the Unified Formulation in terms of a few fundamental nuclei. Formulation with discord interface continuity of transverse stresses and/or electrical displacements are discussed for comparison purpose. We address both equivalent single-layer models and layerwise models; up to fourth-order expansions in the thickness coordinate have been implemented. Numerical analysis has been restricted to closed-form solutions. Plates and simply supported cylindrical shells with orthotropic layers have been investigated. Both sensor and actuator configuration have been analyzed. The results obtained demonstrate the superiority of the proposed approach with respect to the other formulations considered, and its ability to furnish *a priori* interlaminar continuous transverse electrical displacement.

1. Introduction

In recent years piezoelectric materials have been integrated with structural systems to build smart structures which are candidates for next generation of aerospace vehicles, as well as some advanced products in the automotive and ship industries. Piezoelectric materials are, in fact, capable of altering the response of the structures through sensing and actuation. By integrating surface bonded and embedded actuators in structural systems, the desired localized strains may be induced in the structures thanks to the application of an appropriate voltage to the actuators. Reviews on smart materials and structures appear in [Crawley 1994] and [Chopra 2002].

In most applications, the piezoelectric layers are embedded in multilayer structures made of anisotropic composite materials. The efficient use of piezoelectric materials in multilayer structures requires accurate evaluation of mechanical and electric variables in each layer. Classical shell models such as classical lamination theory (CLT) and first-order shear deformation theory (FSDT) can lead to large discrepancies with respect to the exact solution. Improvements can be introduced by using equivalent single-layer models (ESLMs), in which the number of unknown variables is independent of the number of constitutive layers, with higher-order kinematics. However, much better results can be obtained through the use of layerwise models (LWMs), in which the number of unknown variables depends on the number of layers. For recent indications of the superiority of LWMs over ESLMs, see [Robbins and Chopra 2006].

Keywords: piezoelectric shells, unified formulation, closed-form solutions, Reissner Mixed Variational Theorem, interlaminar continuity.

This work has been carried out in the framework of STREP EU project CASSEM under contract NMP-CT-2005-013517.

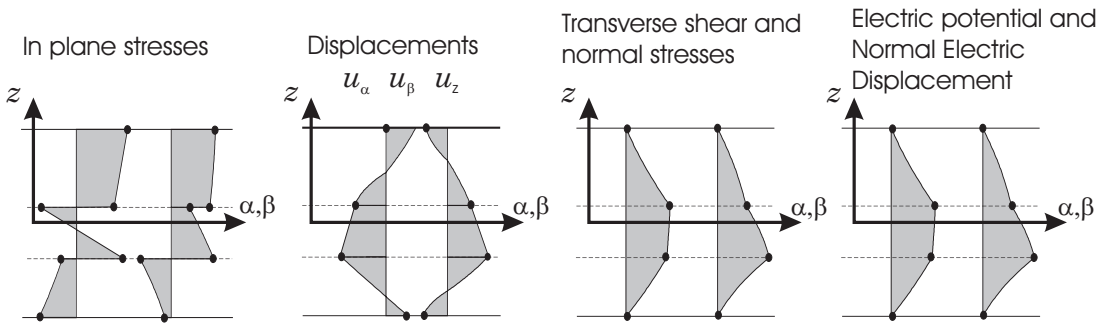

Figure 1. $C^0{}_z$ requirements for the electromechanical case.

The advantages of the Reissner Mixed Variational Theorem (RMVT) with respect to other approaches that mostly make use of the Principle of Virtual Displacement (PVD) were shown in [Carrera 2001; 2003]. The Unified Formulation (UF) was used there to create an hierarchical shell formulation with variable kinematics (relative to displacements and transverse stresses) in each layer. Attention was restricted to pure mechanical problems. UF has been extended to closed-form and finite-element solutions of a piezoelectric plate in [Ballhause et al. 2004] and [Robaldo et al. 2006], respectively; PVD was used and only the displacements and the electrical potential were considered as unknown variables. The main advantage of RMVT is the possibility of fulfilling *a priori* the continuity conditions for the transverse electromechanical variables (electric displacement and stresses). In [Carrera 2001], these continuity conditions have been called C^0_z-requirements. Examples are given in Figure 1, which shows that some variables (mechanical displacements, transverse shear and normal stresses, electric voltage and transverse electrical displacements) must be C^0 continuous in the thickness directions z, while the discontinuity of electromechanical properties at the layer interface requires a discontinuous first derivative of the same variables.

Attempts to introduce the C^0_z-requirements in piezoelectric continua have been made in [D'Ottavio and Kröplin 2006; Carrera and Boscolo 2006]. Closed form and FEs solutions were considered in these last papers, respectively. Attention was restricted to the fulfillment of C^0_z-requirements for transverse shear and normal stress components. Such an extension is herein stated as a "partial" RMVT application. The complete fulfillment of the C^0_z-requirements to both electrical and mechanical variables has been provided in the companion paper [Carrera and Fagiano 2007], devoted to FE analysis and plate geometries.. Such a contribution has been called a "full" extension of RMVT to piezoelectric continua: it allows one to describe *a priori* interlaminar continuous both transverse stresses and transverse electrical displacement component.

A few papers on piezoelectric shells exist in the literature, in particular for the FE method. Layerwise methods were considered in [Heyliger et al. 1996]. FE piezoelectric shells have been considered in [Lammering and Mesecke-Rischmann 2003]. Cho and Roh [2003] proposed geometrically exact shell elements, while Kögl and Bucalem [2005] gave the extension of MITC4 type element to piezoelectric shell structures. Review and assessment have been given in [Saravanos and Heyliger 1999].

Three dimensional piezoelasticity solutions have been addressed in [Wang et al. 2005; Shakeri et al. 2006; Chen et al. 1996; Dumir et al. 1997]. Wang et al. [2005] and Shakeri et al. [2006] dealt with

vibration problems. Chen et al. [1996] addressed cylindrical shell with very thin piezoelectric layers. Only a piezoelectric layer was instead considered in [Dumir et al. 1997]. No results are available in which both mechanical and piezoelectric layers (with thickness comparable to the mechanical layers) are analyzed.

It appears to be of interest to extend the full version of RMVT to piezoelectric shells which is proposed in this work. The present paper could be, in fact, considered as an extension of [Carrera 1999a; 1999b; D'Ottavio et al. 2006; Carrera and Brischetto 2007].

New benchmarks are proposed in this paper related to piezoelectric cylindrical shell that was originally proposed in [Varadan and Bhaskar 1991] for pure mechanical problems. Both actuator and sensor configurations are addressed. The role played by *a priori* continuous $\mathcal{D}_z$ description has been outlined in most of the presented applications.

2. Overview of variational statements

The Principle of Virtual Displacement (PVD) for the pure mechanical static problems, can be written in the form

$$\int_V (\delta\boldsymbol{\epsilon}_{pG}^T\boldsymbol{\sigma}_{pC} + \delta\boldsymbol{\epsilon}_{nG}^T\boldsymbol{\sigma}_{nC})dV = \delta L^e, \tag{1}$$

where $\boldsymbol{u} = (u_\alpha, u_\beta, u_z)$ is the displacement vector; $\boldsymbol{\sigma_p} = (\sigma_{\alpha\alpha}, \sigma_{\beta\beta}, \sigma_{\alpha\beta})$, $\boldsymbol{\sigma_n} = (\sigma_{\alpha z}, \sigma_{\beta z}, \sigma_{zz})$, $\boldsymbol{\epsilon_p} = (\epsilon_{\alpha\alpha}, \epsilon_{\beta\beta}, \epsilon_{\alpha\beta})$ and $\boldsymbol{\epsilon_n} = (\epsilon_{\alpha z}, \epsilon_{\beta z}, \epsilon_{zz})$ are the in-plane and out-plane stresses and strains. The subscript C and G indicate the constitutive equations and the geometrical relations respectively (Sections 4–5).

The Reissner Mixed Variational Theorem assumes both the displacements $\boldsymbol{u}$ and the normal stresses $\boldsymbol{\sigma_n}$ according to the equation

$$\int_V \left(\delta\boldsymbol{\epsilon}_{pG}^T\boldsymbol{\sigma}_{pC} + \delta\boldsymbol{\epsilon}_{nG}^T\boldsymbol{\sigma}_{nM} + \delta\boldsymbol{\sigma}_{nM}^T(\boldsymbol{\epsilon}_{nG} - \boldsymbol{\epsilon}_{nC})\right) dV = \delta L^e. \tag{2}$$

Thus RMVT allows the *a priori* fulfillment of C_z^0-requirements of transverse shear and normal stresses. The subscript M indicates variables assumed from a given model (see Section 6).

The extension of RMVT to piezoelectric case requires the introduction of the internal electric work; see [D'Ottavio and Kröplin 2006; Carrera and Brischetto 2007; Carrera and Boscolo 2006; Garcia Lage et al. 2004]. The primary variables are displacements $\boldsymbol{u}$, normal stresses $\boldsymbol{\sigma_n}$ and electric potential Φ. This extension is referred to as partial P-RMVT:

$$\int_V \left(\delta\boldsymbol{\epsilon}_{pG}^T\boldsymbol{\sigma}_{pC} + \delta\boldsymbol{\epsilon}_{nG}^T\boldsymbol{\sigma}_{nM} + \delta\boldsymbol{\sigma}_{nM}^T(\boldsymbol{\epsilon}_{nG} - \boldsymbol{\epsilon}_{nC}) - \delta\mathcal{E}_G^T\mathcal{D}_C\right) dV = \delta L^e, \tag{3}$$

where $\mathcal{E} = (\mathcal{E}_\alpha, \mathcal{E}_\beta, \mathcal{E}_z)$ is the electric field and $\mathcal{D} = (\mathcal{D}_\alpha, \mathcal{D}_\beta, \mathcal{D}_z)$ is the electric displacement. Applications of P-RMVT to shell were discussed in [Carrera and Brischetto 2007].

The full extension of RMVT to piezomechanical problems (F-RMVT) must consider the transverse electrical displacement $\mathcal{D}_z$ as an additional variable. F-RMVT states that

$$\int_V \left(\delta\boldsymbol{\epsilon}_{pG}^T\boldsymbol{\sigma}_{pC} + \delta\boldsymbol{\epsilon}_{nG}^T\boldsymbol{\sigma}_{nM} - \delta\mathcal{E}_{pG}^T\mathcal{D}_{pC} - \delta\mathcal{E}_{nG}^T\mathcal{D}_{nM} + \delta\boldsymbol{\sigma}_{nM}^T(\boldsymbol{\epsilon}_{nG} - \boldsymbol{\epsilon}_{nC}) - \delta\mathcal{D}_{nM}^T(\mathcal{E}_{nG} - \mathcal{E}_{nC})\right) dV = \delta L^e, \tag{4}$$

where $\mathscr{D}_{\boldsymbol{p}} = (\mathscr{D}_\alpha, \mathscr{D}_\beta)$ and $\mathscr{D}_{\boldsymbol{n}} = (\mathscr{D}_z)$ are in-plane and out-of-plane electric displacements, and $\mathscr{E}_{\boldsymbol{p}} = (\mathscr{E}_\alpha, \mathscr{E}_\beta)$ and $\mathscr{E}_{\boldsymbol{n}} = (\mathscr{E}_z)$ are in-plane and out-of-plane electric fields. F-RMVT allows the complete fulfillment of C_z^0-requirements.

Appropriate "constitutive" equations are required for (1)–(4), as discussed in Section 5.

3. Shell geometry

Geometry and notation for multilayer shells are shown in Figure 2; for details see [Rogacheva 1994]. The square of an infinitesimal linear segment in the layer, the associated infinitesimal area and volume elements are given by

$$\begin{aligned} ds_k^2 &= H_\alpha^{k^2}\, d\alpha_k^2 + H_\beta^{k^2}\, d\beta_k^2 + H_z^{k^2}\, dz_k^2, \\ d\Omega_k &= H_\alpha^k H_\beta^k\, d\alpha_k\, d\beta_k, \qquad dV = H_\alpha^k\, H_\beta^k\, H_z^k\, d\alpha_k\, d\beta_k\, dz_k, \end{aligned} \tag{5}$$

where the metric coefficients are

$$H_\alpha^k = A^k(1 + z_k/R_\alpha^k), \qquad H_\beta^k = B^k(1 + z_k/R_\beta^k), \qquad H_z^k = 1, \tag{6}$$

k is the layer index in the multilayer shell, and R_α^k and R_β^k are the principal radii of curvature along the coordinates α_k and β_k. A^k and B^k are the coefficients of the first fundamental form of Ω_k (Γ_k is the Ω_k boundary). In this paper, the attention has been restricted to shells with constant radii of curvature (cylindrical, spherical, toroidal geometries) for which $A^k = B^k = 1$.

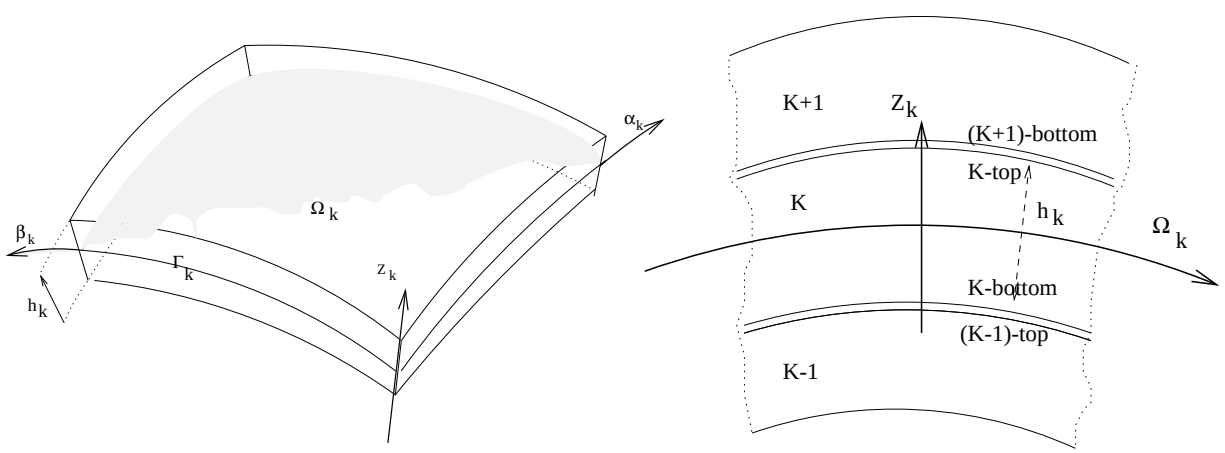

Figure 2. Geometry and notation for the layered shell.

4. Geometrical relations

The geometrical relations allow one to express the in-plane strain $\boldsymbol{\epsilon_p}$ and out-of-plane strain $\boldsymbol{\epsilon_n}$ in terms of displacement $\boldsymbol{u}$. At the same way the in-plane components $\mathscr{E}_{\boldsymbol{p}}$ and out-of-plane components $\mathscr{E}_{\boldsymbol{n}}$ of electric field can be expressed in terms of the electric potential $\boldsymbol{\Phi}$. Then

$$\begin{aligned} \boldsymbol{\epsilon}_{pG} &= [\epsilon_{\alpha\alpha}, \epsilon_{\beta\beta}, \epsilon_{\alpha\beta}]^T = (\boldsymbol{D}_p + \boldsymbol{A}_p)\, \boldsymbol{u}, \qquad & \boldsymbol{\epsilon}_{nG} &= [\epsilon_{\alpha z}, \epsilon_{\beta z}, \epsilon_{zz}]^T = (\boldsymbol{D}_{n\Omega} + \boldsymbol{D}_{nz} - \boldsymbol{A}_n)\, \boldsymbol{u}, \\ \mathscr{E}_{pG} &= [\mathscr{E}_\alpha, \mathscr{E}_\beta]^T = -\boldsymbol{D}_{e\Omega}\, \boldsymbol{\Phi}, & \mathscr{E}_{nG} &= [\mathscr{E}_z]^T = -\boldsymbol{D}_{en}\, \boldsymbol{\Phi}. \end{aligned} \tag{7}$$

The explicit form of the introduced arrays follows:

$$\boldsymbol{D}_p = \begin{bmatrix} \partial_\alpha/H_\alpha & 0 & 0 \\ 0 & \partial_\beta/H_\beta & 0 \\ \partial_\beta/H_\beta & \partial_\alpha/H_\alpha & 0 \end{bmatrix}, \quad \boldsymbol{D}_{n\Omega} = \begin{bmatrix} 0 & 0 & \partial_\alpha/H_\alpha \\ 0 & 0 & \partial_\beta/H_\beta \\ 0 & 0 & 0 \end{bmatrix}, \quad \boldsymbol{D}_{nz} = \begin{bmatrix} \partial_z & 0 & 0 \\ 0 & \partial_z & 0 \\ 0 & 0 & \partial_z \end{bmatrix},$$

$$\boldsymbol{D}_{e\Omega} = \begin{bmatrix} \partial_\alpha/H_\alpha & 0 & 0 \\ 0 & \partial_\beta/H_\beta & 0 \\ 0 & 0 & 0 \end{bmatrix}, \quad \boldsymbol{D}_{en} = \begin{bmatrix} 0 & 0 & 0 \\ 0 & 0 & 0 \\ 0 & 0 & \partial_z \end{bmatrix},$$

$$\boldsymbol{A}_p = \begin{bmatrix} 0 & 0 & 1/(H_\alpha R_\alpha) \\ 0 & 0 & 1/(H_\beta R_\beta) \\ 0 & 0 & 0 \end{bmatrix}, \quad \boldsymbol{A}_n = \begin{bmatrix} 1/(H_\alpha R_\alpha) & 0 & 0 \\ 0 & 1/(H_\beta R_\beta) & 0 \\ 0 & 0 & 0 \end{bmatrix}.$$

For convenience, the electric potential, the in-plane and out-of-plane electric field have been treated as the $[3 \times 1]$ vector with components $\boldsymbol{\Phi} = (\Phi, \Phi, \Phi)$, $\mathscr{E}_{pG} = (\mathscr{E}_\alpha, \mathscr{E}_\beta, \mathscr{E}_\beta)$, $\mathscr{E}_{nG} = (\mathscr{E}_z, \mathscr{E}_z, \mathscr{E}_z)$. Such an artifice will allow us to preserve the $[3 \times 3]$ dimension for the fundamental nuclei.

5. Constitutive equations

The constitutive equations of a piezoelectric continuum can be written in various forms; see [Ikeda 1996; Rogacheva 1994]. Different choices lead to the use of different electromechanical coefficients and field variables. The two most used forms are related to the Gibbs free energy G and the electric Gibbs energy G_2, respectively. These are often referred to as the d-form and the e-form, [Carrera and Brischetto 2007]. The formulation based on G_2 is used in this work; we will present the constitutive equations for the PVD formulation and their split form in in-plane and out-of-plane components. We then use these equations to obtain the constitutive equations which are consistent with F-RMVT application.

Classical PVD formulation. The displacement $\boldsymbol{u}$ and the potential $\boldsymbol{\Phi}$ are the unknown variables in the PVD setting. The electric Gibbs energy G_2 is (see [Carrera and Brischetto 2007])

$$G_2(\boldsymbol{\epsilon}, \mathscr{E}) = \tfrac{1}{2}\boldsymbol{\epsilon}^T \boldsymbol{C}^{\mathscr{E}} \boldsymbol{\epsilon} - \tfrac{1}{2}\mathscr{E}^T \boldsymbol{\varepsilon}^{\epsilon} \mathscr{E} - \mathscr{E}^T \boldsymbol{e}\boldsymbol{\epsilon}, \tag{8}$$

in which $\boldsymbol{C}^{\mathscr{E}}$ is the elastic coefficients matrix related to constant electric field. The $[6 \times 6]$ matrix $\boldsymbol{C}$ of an orthotropic material in the rotated reference system assumes the form (see [Reddy 2004])

$$\boldsymbol{C}^{\mathscr{E}} = \begin{bmatrix} C_{11} & C_{12} & C_{16} & 0 & 0 & C_{13} \\ C_{12} & C_{22} & C_{26} & 0 & 0 & C_{23} \\ C_{16} & C_{26} & C_{66} & 0 & 0 & C_{63} \\ 0 & 0 & 0 & C_{55} & C_{45} & 0 \\ 0 & 0 & 0 & C_{45} & C_{44} & 0 \\ C_{31} & C_{32} & C_{36} & 0 & 0 & C_{33} \end{bmatrix} = \begin{bmatrix} \boldsymbol{C}^{\mathscr{E}}_{pp} & \boldsymbol{C}^{\mathscr{E}}_{pn} \\ \boldsymbol{C}^{\mathscr{E}}_{np} & \boldsymbol{C}^{\mathscr{E}}_{nn} \end{bmatrix}, \tag{9}$$

$\boldsymbol{C}^{\mathscr{E}}_{pp}$, $\boldsymbol{C}^{\mathscr{E}}_{pn}$, $\boldsymbol{C}^{\mathscr{E}}_{np}$ and $\boldsymbol{C}^{\mathscr{E}}_{nn}$ are $[3 \times 3]$ submatrices related to in-plane p and out-of-plane (normal n) strain/stress components.

The piezoelectric and dielectric coefficient matrices are

$$\boldsymbol{e} = \begin{bmatrix} 0 & 0 & 0 & e_{15} & e_{14} & 0 \\ 0 & 0 & 0 & e_{25} & e_{24} & 0 \\ e_{31} & e_{32} & e_{36} & 0 & 0 & e_{33} \end{bmatrix}, \quad \boldsymbol{\varepsilon}^{\epsilon} = \begin{bmatrix} \varepsilon_{11}^{\epsilon} & \varepsilon_{12}^{\epsilon} & 0 \\ \varepsilon_{21}^{\epsilon} & \varepsilon_{22}^{\epsilon} & 0 \\ 0 & 0 & \varepsilon_{33}^{\epsilon} \end{bmatrix}, \tag{10}$$

where the dielectric coefficients refer to a constant strain state, $\mathscr{E}$ is the electric field, $\boldsymbol{\epsilon}$ is the $[6 \times 1]$ strain vector with components $\boldsymbol{\epsilon} = (\epsilon_{\alpha\alpha}, \epsilon_{\beta\beta}, \epsilon_{\alpha\beta}, \epsilon_{\alpha z}, \epsilon_{\beta z}, \epsilon_{zz})$.

The stresses $\boldsymbol{\sigma} = (\sigma_{\alpha\alpha}, \sigma_{\beta\beta}, \sigma_{\alpha\beta}, \sigma_{\alpha z}, \sigma_{\beta z}, \sigma_{zz})$ and electrical displacements $\mathscr{D}$ are obtained upon direct differentiation of G_2:

$$\begin{aligned} \boldsymbol{\sigma} &= \frac{\partial G_2}{\partial \boldsymbol{\epsilon}} = \frac{\partial}{\partial \boldsymbol{\epsilon}}\left(\tfrac{1}{2}\boldsymbol{\epsilon}^T \boldsymbol{C}^{\mathscr{E}} \boldsymbol{\epsilon} - \tfrac{1}{2}\mathscr{E}^T \boldsymbol{\varepsilon}^{\epsilon} \mathscr{E} - \mathscr{E}^T \boldsymbol{e}\boldsymbol{\epsilon}\right) = \boldsymbol{C}^{\mathscr{E}}\boldsymbol{\epsilon} - \boldsymbol{e}^T \mathscr{E}, \\ \mathscr{D} &= -\frac{\partial G_2}{\partial \mathscr{E}} = -\frac{\partial}{\partial \mathscr{E}}\left(\tfrac{1}{2}\boldsymbol{\epsilon}^T \boldsymbol{C}^{\mathscr{E}} \boldsymbol{\epsilon} - \tfrac{1}{2}\mathscr{E}^T \boldsymbol{\varepsilon}^{\epsilon} \mathscr{E} - \mathscr{E}^T \boldsymbol{e}\boldsymbol{\epsilon}\right) = \boldsymbol{e}\boldsymbol{\epsilon} + \boldsymbol{\varepsilon}^{\epsilon}\mathscr{E}. \end{aligned} \tag{11}$$

The corresponding $\boldsymbol{e}$-form of the constitutive equations is split into in-plane and out-of-plane components:

$$\begin{aligned} \boldsymbol{\sigma_p} &= \frac{\partial G_2}{\partial \boldsymbol{\epsilon_p}} = \boldsymbol{C}_{\boldsymbol{pp}}^{\mathscr{E}}\boldsymbol{\epsilon_p} + \boldsymbol{C}_{\boldsymbol{pn}}^{\mathscr{E}}\boldsymbol{\epsilon_n} - \boldsymbol{e}_{pp}^T \mathscr{E}_{\boldsymbol{p}} - \boldsymbol{e}_{np}^T \mathscr{E}_{\boldsymbol{n}}, \\ \boldsymbol{\sigma_n} &= \frac{\partial G_2}{\partial \boldsymbol{\epsilon_n}} = \boldsymbol{C}_{\boldsymbol{np}}^{\mathscr{E}}\boldsymbol{\epsilon_p} + \boldsymbol{C}_{\boldsymbol{nn}}^{\mathscr{E}}\boldsymbol{\epsilon_n} - \boldsymbol{e}_{pn}^T \mathscr{E}_{\boldsymbol{p}} - \boldsymbol{e}_{nn}^T \mathscr{E}_{\boldsymbol{n}}, \\ \mathscr{D}_{\boldsymbol{p}} &= -\frac{\partial G_2}{\partial \mathscr{E}_{\boldsymbol{p}}} = \boldsymbol{e}_{\boldsymbol{pp}}\boldsymbol{\epsilon_p} + \boldsymbol{e}_{\boldsymbol{pn}}\boldsymbol{\epsilon_n} + \boldsymbol{\varepsilon}_{pp}^{\epsilon}\mathscr{E}_{\boldsymbol{p}} + \boldsymbol{\varepsilon}_{pn}^{\epsilon}\mathscr{E}_{\boldsymbol{n}}, \\ \mathscr{D}_{\boldsymbol{n}} &= -\frac{\partial G_2}{\partial \mathscr{E}_{\boldsymbol{n}}} = \boldsymbol{e}_{\boldsymbol{np}}\boldsymbol{\epsilon_p} + \boldsymbol{e}_{\boldsymbol{nn}}\boldsymbol{\epsilon_n} + \boldsymbol{\varepsilon}_{np}^{\epsilon}\mathscr{E}_{\boldsymbol{p}} + \boldsymbol{\varepsilon}_{nn}^{\epsilon}\mathscr{E}_{\boldsymbol{n}}, \end{aligned} \tag{12}$$

where

$$\boldsymbol{e}_{pp} = \begin{bmatrix} 0 & 0 & 0 \\ 0 & 0 & 0 \end{bmatrix}, \quad \boldsymbol{e}_{pn} = \begin{bmatrix} e_{15} & e_{14} & 0 \\ e_{25} & e_{24} & 0 \end{bmatrix}, \quad \boldsymbol{e}_{np} = \begin{bmatrix} e_{31} & e_{32} & e_{36} \end{bmatrix}, \quad \boldsymbol{e}_{nn} = \begin{bmatrix} 0 & 0 & e_{33} \end{bmatrix},$$

$$\boldsymbol{\varepsilon}_{pp} = \begin{bmatrix} \varepsilon_{11} & \varepsilon_{12} \\ \varepsilon_{12} & \varepsilon_{22} \end{bmatrix}, \quad \boldsymbol{\varepsilon}_{pn} = \begin{bmatrix} 0 \\ 0 \end{bmatrix}, \quad \boldsymbol{\varepsilon}_{np} = \begin{bmatrix} 0 & 0 \end{bmatrix}, \quad \boldsymbol{\varepsilon}_{nn} = \begin{bmatrix} \varepsilon_{33} \end{bmatrix}.$$

F-RMVT constitutive equations. In the F-RMVT setting one assumes the displacement $\boldsymbol{u}$, electric potential $\boldsymbol{\Phi}$, transverse stresses $\boldsymbol{\sigma_n}$ and normal electric displacement $\mathscr{D}_{\boldsymbol{n}}$. The correspondent constitutive equations are

$$\begin{aligned} \boldsymbol{\sigma_p} &= \boldsymbol{C}_{\boldsymbol{\sigma\mathscr{D}}}\mathscr{D}_{\boldsymbol{n}} + \boldsymbol{C}_{\boldsymbol{\sigma\epsilon}}\boldsymbol{\epsilon_p} + \boldsymbol{C}_{\boldsymbol{\sigma\sigma}}\boldsymbol{\sigma_n} + \boldsymbol{C}_{\boldsymbol{\sigma\mathscr{E}}}\mathscr{E}_{\boldsymbol{p}}, \\ \boldsymbol{\epsilon_n} &= \boldsymbol{C}_{\boldsymbol{\epsilon\mathscr{D}}}\mathscr{D}_{\boldsymbol{n}} + \boldsymbol{C}_{\boldsymbol{\epsilon\epsilon}}\boldsymbol{\epsilon_p} + \boldsymbol{C}_{\boldsymbol{\epsilon\sigma}}\boldsymbol{\sigma_n} + \boldsymbol{C}_{\boldsymbol{\epsilon\mathscr{E}}}\mathscr{E}_{\boldsymbol{p}}, \\ \mathscr{D}_{\boldsymbol{p}} &= \boldsymbol{C}_{\boldsymbol{\mathscr{D}\mathscr{D}}}\mathscr{D}_{\boldsymbol{n}} + \boldsymbol{C}_{\boldsymbol{\mathscr{D}\epsilon}}\boldsymbol{\epsilon_p} + \boldsymbol{C}_{\boldsymbol{\mathscr{D}\sigma}}\boldsymbol{\sigma_n} + \boldsymbol{C}_{\boldsymbol{\mathscr{D}\mathscr{E}}}\mathscr{E}_{\boldsymbol{p}}, \\ \mathscr{E}_{\boldsymbol{n}} &= \boldsymbol{C}_{\boldsymbol{\mathscr{E}\mathscr{D}}}\mathscr{D}_{\boldsymbol{n}} + \boldsymbol{C}_{\boldsymbol{\mathscr{E}\epsilon}}\boldsymbol{\epsilon_p} + \boldsymbol{C}_{\boldsymbol{\mathscr{E}\sigma}}\boldsymbol{\sigma_n} + \boldsymbol{C}_{\boldsymbol{\mathscr{E}\mathscr{E}}}\mathscr{E}_{\boldsymbol{p}}, \end{aligned} \tag{13}$$

in which in-plane strains and electrical field components as well as transverse stresses and transverse electrical displacement are used to express $\boldsymbol{\sigma_p}$, $\boldsymbol{\epsilon_n}$, $\mathscr{D}_{\boldsymbol{p}}$ and $\mathscr{E}_{\boldsymbol{n}}$ as requested by F-RMVT in Equation (4).

The explicit forms of the matrices in Equation (13) are

$$
\begin{aligned}
\boldsymbol{C}_{\sigma\mathscr{D}} &= (\boldsymbol{C}_{pn}\boldsymbol{C}_{nn}^{-1}\boldsymbol{e}_{nn}^T - \boldsymbol{e}_{np}^T)(\boldsymbol{e}_{nn}\boldsymbol{C}_{nn}^{-1}\boldsymbol{e}_{nn}^T + \boldsymbol{\varepsilon}_{nn})^{-1},\\
\boldsymbol{C}_{\sigma\epsilon} &= \boldsymbol{C}_{pp} - \boldsymbol{C}_{pn}\boldsymbol{C}_{nn}^{-1}\boldsymbol{C}_{np} - (\boldsymbol{C}_{pn}\boldsymbol{C}_{nn}^{-1}\boldsymbol{e}_{nn}^T - \boldsymbol{e}_{np}^T)(\boldsymbol{e}_{nn}\boldsymbol{C}_{nn}^{-1}\boldsymbol{e}_{nn}^T + \boldsymbol{\varepsilon}_{nn})^{-1}(\boldsymbol{e}_{np} - \boldsymbol{e}_{nn}\boldsymbol{C}_{nn}^{-1}\boldsymbol{C}_{np}),\\
\boldsymbol{C}_{\sigma\sigma} &= \boldsymbol{C}_{pn}\boldsymbol{C}_{nn}^{-1} - (\boldsymbol{C}_{pn}\boldsymbol{C}_{nn}^{-1}\boldsymbol{e}_{nn}^T - \boldsymbol{e}_{np}^T)(\boldsymbol{e}_{nn}\boldsymbol{C}_{nn}^{-1}\boldsymbol{e}_{nn}^T + \boldsymbol{\varepsilon}_{nn})^{-1}\boldsymbol{e}_{nn}\boldsymbol{C}_{nn}^{-1},\\
\boldsymbol{C}_{\sigma\mathscr{E}} &= \boldsymbol{C}_{pn}\boldsymbol{C}_{nn}^{-1}\boldsymbol{e}_{pn}^T - \boldsymbol{e}_{pp}^T - (\boldsymbol{C}_{pn}\boldsymbol{C}_{nn}^{-1}\boldsymbol{e}_{nn}^T - \boldsymbol{e}_{np}^T)(\boldsymbol{e}_{nn}\boldsymbol{C}_{nn}^{-1}\boldsymbol{e}_{nn}^T + \boldsymbol{\varepsilon}_{nn})^{-1}(\boldsymbol{e}_{nn}\boldsymbol{C}_{nn}^{-1}\boldsymbol{e}_{pn}^T + \boldsymbol{\varepsilon}_{np}),\\
\boldsymbol{C}_{\epsilon\mathscr{D}} &= \boldsymbol{C}_{nn}^{-1}\boldsymbol{e}_{nn}^T(\boldsymbol{e}_{nn}\boldsymbol{C}_{nn}^{-1}\boldsymbol{e}_{nn}^T + \boldsymbol{\varepsilon}_{nn})^{-1},\\
\boldsymbol{C}_{\epsilon\epsilon} &= -\boldsymbol{C}_{nn}^{-1}\boldsymbol{C}_{np} - \boldsymbol{C}_{nn}^{-1}\boldsymbol{e}_{nn}^T(\boldsymbol{e}_{nn}\boldsymbol{C}_{nn}^{-1}\boldsymbol{e}_{nn}^T + \boldsymbol{\varepsilon}_{nn})^{-1}(\boldsymbol{e}_{np} - \boldsymbol{e}_{nn}\boldsymbol{C}_{nn}^{-1}\boldsymbol{C}_{np}),\\
\boldsymbol{C}_{\epsilon\sigma} &= \boldsymbol{C}_{nn}^{-1} - \boldsymbol{C}_{nn}^{-1}\boldsymbol{e}_{nn}^T(\boldsymbol{e}_{nn}\boldsymbol{C}_{nn}^{-1}\boldsymbol{e}_{nn}^T + \boldsymbol{\varepsilon}_{nn})^{-1}\boldsymbol{e}_{nn}\boldsymbol{C}_{nn}^{-1},\\
\boldsymbol{C}_{\epsilon\mathscr{E}} &= \boldsymbol{C}_{nn}^{-1}\boldsymbol{e}_{pn}^T - \boldsymbol{C}_{nn}^{-1}\boldsymbol{e}_{nn}^T(\boldsymbol{e}_{nn}\boldsymbol{C}_{nn}^{-1}\boldsymbol{e}_{nn}^T + \boldsymbol{\varepsilon}_{nn})^{-1}(\boldsymbol{e}_{nn}\boldsymbol{C}_{nn}^{-1}\boldsymbol{e}_{pn}^T + \boldsymbol{\varepsilon}_{np}),\\
\boldsymbol{C}_{\mathscr{D}\mathscr{D}} &= \boldsymbol{e}_{pn}\boldsymbol{C}_{nn}^{-1}\boldsymbol{e}_{nn}^T(\boldsymbol{e}_{nn}\boldsymbol{C}_{nn}^{-1}\boldsymbol{e}_{nn}^T + \boldsymbol{\varepsilon}_{nn})^{-1} + \boldsymbol{\varepsilon}_{pn}(\boldsymbol{e}_{nn}\boldsymbol{C}_{nn}^{-1}\boldsymbol{e}_{nn}^T + \boldsymbol{\varepsilon}_{nn})^{-1},\\
\boldsymbol{C}_{\mathscr{D}\epsilon} &= \boldsymbol{e}_{pp} - \boldsymbol{e}_{pn}\boldsymbol{C}_{nn}^{-1}\boldsymbol{C}_{np} - (\boldsymbol{e}_{pn}\boldsymbol{C}_{nn}^{-1}\boldsymbol{e}_{nn}^T + \boldsymbol{\varepsilon}_{pn})(\boldsymbol{e}_{nn}\boldsymbol{C}_{nn}^{-1}\boldsymbol{e}_{nn}^T + \boldsymbol{\varepsilon}_{nn})^{-1}(\boldsymbol{e}_{np} - \boldsymbol{e}_{nn}\boldsymbol{C}_{nn}^{-1}\boldsymbol{C}_{np}),\\
\boldsymbol{C}_{\mathscr{D}\sigma} &= \boldsymbol{e}_{pn}\boldsymbol{C}_{nn}^{-1} - \boldsymbol{e}_{pn}\boldsymbol{C}_{nn}^{-1}\boldsymbol{e}_{nn}^T(\boldsymbol{e}_{nn}\boldsymbol{C}_{nn}^{-1}\boldsymbol{e}_{nn}^T + \boldsymbol{\varepsilon}_{nn})^{-1}\boldsymbol{e}_{nn}\boldsymbol{C}_{nn}^{-1} - \boldsymbol{\varepsilon}_{pn}(\boldsymbol{e}_{nn}\boldsymbol{C}_{nn}^{-1}\boldsymbol{e}_{nn}^T + \boldsymbol{\varepsilon}_{nn})^{-1}\boldsymbol{e}_{nn}\boldsymbol{C}_{nn}^{-1},\\
\boldsymbol{C}_{\mathscr{D}\mathscr{E}} &= \boldsymbol{e}_{pn}\boldsymbol{C}_{nn}^{-1}\boldsymbol{e}_{pn}^T - (\boldsymbol{e}_{pn}\boldsymbol{C}_{nn}^{-1}\boldsymbol{e}_{nn}^T + \boldsymbol{\varepsilon}_{pn})(\boldsymbol{e}_{nn}\boldsymbol{C}_{nn}^{-1}\boldsymbol{e}_{nn}^T + \boldsymbol{\varepsilon}_{nn})^{-1}(\boldsymbol{e}_{nn}\boldsymbol{C}_{nn}^{-1}\boldsymbol{e}_{pn}^T + \boldsymbol{\varepsilon}_{np}) + \boldsymbol{\varepsilon}_{pp},\\
\boldsymbol{C}_{\mathscr{E}\mathscr{D}} &= (\boldsymbol{e}_{nn}\boldsymbol{C}_{nn}^{-1}\boldsymbol{e}_{nn}^T + \boldsymbol{\varepsilon}_{nn})^{-1},\\
\boldsymbol{C}_{\mathscr{E}\epsilon} &= -(\boldsymbol{e}_{nn}\boldsymbol{C}_{nn}^{-1}\boldsymbol{e}_{nn}^T + \boldsymbol{\varepsilon}_{nn})^{-1}(\boldsymbol{e}_{np} - \boldsymbol{e}_{nn}\boldsymbol{C}_{nn}^{-1}\boldsymbol{C}_{np}),\\
\boldsymbol{C}_{\mathscr{E}\sigma} &= -(\boldsymbol{e}_{nn}\boldsymbol{C}_{nn}^{-1}\boldsymbol{e}_{nn}^T + \boldsymbol{\varepsilon}_{nn})^{-1}\boldsymbol{e}_{nn}\boldsymbol{C}_{nn}^{-1},\\
\boldsymbol{C}_{\mathscr{E}\mathscr{E}} &= -(\boldsymbol{e}_{nn}\boldsymbol{C}_{nn}^{-1}\boldsymbol{e}_{nn}^T + \boldsymbol{\varepsilon}_{nn})^{-1}(\boldsymbol{e}_{nn}\boldsymbol{C}_{nn}^{-1}\boldsymbol{e}_{pn}^T + \boldsymbol{\varepsilon}_{np}).
\end{aligned}
\tag{14}
$$

6. Unified formulation for shell theories

The Unified Formulation is a technique that allows one to handle in a unified manner a large variety of plate/shell modelings. According to UF, the governing equations are written in term of a few *fundamental nuclei*, which do not formally depend on the expansion N used in the z-direction, or in the variable description (LW or ESL).

The unknown variables $\boldsymbol{u}$, $\boldsymbol{\sigma}_n$, Φ and $\mathscr{D}_n$ are expressed in term of the layer thickness coordinate as

$$
\begin{aligned}
&\big(\boldsymbol{u}^k(x,y,z),\Phi^k(x,y,z),\boldsymbol{\sigma}_n^k(x,y,z),\mathscr{D}_n^k(x,y,z)\big) = F_b(z)\big(\boldsymbol{u}_b^k(x,y),\Phi_b^k(x,y),\boldsymbol{\sigma}_{nb}^k(x,y),\mathscr{D}_{nb}^k(x,y)\big)\\
&\quad + F_r(z)\big(\boldsymbol{u}_r^k(x,y),\Phi_r^k(x,y),\boldsymbol{\sigma}_{nr}^k(x,y),\mathscr{D}_{nr}^k(x,y)\big) + F_t(z)\big(\boldsymbol{u}_t^k(x,y),\Phi_t^k(x,y),\boldsymbol{\sigma}_{nt}^k(x,y),\mathscr{D}_{nt}^k(x,y)\big)
\end{aligned}
\tag{15}
$$

The subscript t and b denote the linear part of the thickness expansion (t and b will be used to denote top- and bottom-layer variable values in layerwise cases), while subscript r refers to higher-order terms: $r = 1, \ldots, N-1$. In compact form,

$$
\big(\boldsymbol{u}^k(x,y,z),\Phi^k(x,y,z),\boldsymbol{\sigma}_n^k(x,y,z),\mathscr{D}_n^k(x,y,z)\big) = F_\tau(z)\big(\boldsymbol{u}^k(x,y),\Phi^k(x,y),\boldsymbol{\sigma}_n^k(x,y),\mathscr{D}_n^k(x,y)\big)_\tau. \tag{16}
$$

Here $\big(\boldsymbol{u}^k(x,y), \Phi^k(x,y), \boldsymbol{\sigma}_n^k(x,y), \mathscr{D}_n^k(x,y)\big)_\tau$ are two-dimensional unknowns, the $F_\tau(z)$ are the base functions of the expansion, and the summation convention over repeated indices has been adopted. The base functions could be, in general, different for each variable. Different choices for $F_\tau(z)$ will lead

to different plate/shell theories. The choices made in our study are briefly discussed below; detailed descriptions can be found in the works cited.

Layerwise models. The thickness functions are given by combinations of Legendre polynomials P_j as

$$F_t = \frac{P_0(\zeta_k) + P_1(\zeta_k)}{2}, \quad F_b = \frac{P_0(\zeta_k) - P_1(\zeta_k)}{2}, \quad F_r = P_r(\zeta_k) - P_{r-2}(\zeta_k), \quad r = 2, 3, \ldots, N, \tag{17}$$

for $\zeta = z_k/2h_k$, where z_k is the local layer thickness coordinate and h_k is the layer thickness, so $-1 \leq \zeta_k \leq 1$. As mentioned, t and b denote top and bottom; that is, the chosen functions have the properties

$$\zeta_k = \begin{cases} 1 \ : \ F_t = 1, \ \ F_b = 0, \ \ F_r = 0, \\ -1 \ : \ F_t = 0, \ \ F_b = 1, \ \ F_r = 0, \end{cases} \tag{18}$$

Thanks to these properties the interlaminar continuity of the assumed variables can be easily linked in the assembly procedure from layer-level matrices to multilayer-level matrices.

Equivalent single-layer model. In this case the layerwise expansion is preserved for the transverse stresses, electric potential and electric displacements, while a Taylor-type expansion is used for the displacement components:

$$\boldsymbol{u}(x, y, z) = \boldsymbol{u}_\tau(x, y)\, z^\tau, \quad \tau = 0, N.$$

The base functions related to displacements can be chosen as

$$F_b(z) = 1, \quad F_r(z) = z^r, \ \ r = 1, \ldots, N-1, \quad F_t(z) = z^N.$$

A refinement of the ESL formulation can be reached by adding to the displacement assumption a function that imposes a zigzag form onto the displacement distribution. Following Murakami [1986], who introduced this idea, we take the displacement with imposed zigzag as

$$\boldsymbol{u} = \boldsymbol{u}_0 + (-1)^k \zeta_k \boldsymbol{u}_Z + z^r \boldsymbol{u}_r, \quad r = 1, \ldots, N-1. \tag{19}$$

The zigzag term, denoted by the subscript Z, changes sign for each layer k. These terms can be represented in unified form, by referring the subscript t to the zigzag function: $\boldsymbol{u}_t = \boldsymbol{u}_Z$. In this case, the thickness functions are defined as

$$F_b = 1, \qquad F_t = (-1)^k \zeta_k, \qquad F_r = z^r \quad \text{for } r = 1, \ldots, N-1. \tag{20}$$

These ESLM with zigzag functions are considered with linear, parabolic and cubic expansions.

7. Governing equations

Upon substitution of the constitutive equation (13), the geometrical relations (7) and Equation (16) in Equation (4), and after integration by parts (see [Carrera 1998; 1999a; 1999b]), we obtain the governing differential equations for the piezoelectric layers consistent with the assumptions made.

The electromechanical equilibrium and compatibility equations on the domain Ω^k are

$$\begin{aligned}
\delta \boldsymbol{u}_\tau^k &: \boldsymbol{K}_{uu}^{k\tau s}\boldsymbol{u}_s^k + \boldsymbol{K}_{u\sigma}^{k\tau s}(\boldsymbol{\sigma}_n^k)_s + \boldsymbol{K}_{ue}^{k\tau s}\boldsymbol{\Phi}_s^k + \boldsymbol{K}_{u\mathscr{D}}^{k\tau s}(\mathscr{D}_{\boldsymbol{n}}^{\boldsymbol{k}})_s = \boldsymbol{p}_\tau^k,\\
\delta(\boldsymbol{\sigma}_n^k)_\tau &: \boldsymbol{K}_{\sigma u}^{k\tau s}\boldsymbol{u}_s^k + \boldsymbol{K}_{\sigma\sigma}^{k\tau s}(\boldsymbol{\sigma}_n^k)_s + \boldsymbol{K}_{\sigma e}^{k\tau s}\boldsymbol{\Phi}_s^k + \boldsymbol{K}_{\sigma\mathscr{D}}^{k\tau s}(\mathscr{D}_{\boldsymbol{n}}^{\boldsymbol{k}})_s = 0,\\
\delta\boldsymbol{\Phi}_\tau^k &: \boldsymbol{K}_{eu}^{k\tau s}\boldsymbol{u}_s^k + \boldsymbol{K}_{e\sigma}^{k\tau s}(\boldsymbol{\sigma}_n^k)_s + \boldsymbol{K}_{ee}^{k\tau s}\boldsymbol{\Phi}_s^k + \boldsymbol{K}_{e\mathscr{D}}^{k\tau s}(\mathscr{D}_{\boldsymbol{n}}^{\boldsymbol{k}})_s = \boldsymbol{p}_{e\tau}^k,\\
\delta(\mathscr{D}_n^k)_\tau &: \boldsymbol{K}_{\mathscr{D}u}^{k\tau s}\boldsymbol{u}_s^k + \boldsymbol{K}_{\mathscr{D}\sigma}^{k\tau s}(\boldsymbol{\sigma}_n^k)_s + \boldsymbol{K}_{\mathscr{D}e}^{k\tau s}\boldsymbol{\Phi}_s^k + \boldsymbol{K}_{\mathscr{D}\mathscr{D}}^{k\tau s}(\mathscr{D}_{\boldsymbol{n}}^{\boldsymbol{k}})_s = 0.
\end{aligned} \tag{21}$$

Two types of boundary conditions on Γ^k are obtained: those of the Dirichlet type,

$$\boldsymbol{u}_s^k = \bar{\boldsymbol{u}}_s^k, \quad \boldsymbol{\Phi}_s^k = \overline{\boldsymbol{\Phi}}_s^k, \tag{22}$$

and those of Neumann type,

$$\begin{aligned}
\boldsymbol{\Pi}_{uu}^{k\tau s}\boldsymbol{u}_s^k + \boldsymbol{\Pi}_{u\sigma}^{k\tau s}(\boldsymbol{\sigma}_n^k)_s + \boldsymbol{\Pi}_{ue}^{k\tau s}\boldsymbol{\Phi}_s^k + \boldsymbol{\Pi}_{u\mathscr{D}}^{k\tau s}(\mathscr{D}_n^k)_s &= \boldsymbol{\Pi}_{uu}^{k\tau s}\bar{\boldsymbol{u}}_s^k + \boldsymbol{\Pi}_{u\sigma}^{k\tau s}(\overline{\boldsymbol{\sigma}}_n^k)_s + \boldsymbol{\Pi}_{ue}^{k\tau s}\overline{\boldsymbol{\Phi}}_s^k + \boldsymbol{\Pi}_{u\mathscr{D}}^{k\tau s}(\overline{\mathscr{D}}_n^k)_s,\\
\boldsymbol{\Pi}_{eu}^{k\tau s}\boldsymbol{u}_s^k + \boldsymbol{\Pi}_{e\sigma}^{k\tau s}(\boldsymbol{\sigma}_n^k)_s + \boldsymbol{\Pi}_{ee}^{k\tau s}\boldsymbol{\Phi}_s^k + \boldsymbol{\Pi}_{e\mathscr{D}}^{k\tau s}(\mathscr{D}_n^k)_s &= \boldsymbol{\Pi}_{eu}^{k\tau s}\bar{\boldsymbol{u}}_s^k + \boldsymbol{\Pi}_{e\sigma}^{k\tau s}(\overline{\boldsymbol{\sigma}}_n^k)_s + \boldsymbol{\Pi}_{ee}^{k\tau s}\overline{\boldsymbol{\Phi}}_s^k + \boldsymbol{\Pi}_{e\mathscr{D}}^{k\tau s}(\overline{\mathscr{D}}_n^k)_s.
\end{aligned} \tag{23}$$

The *fundamental nuclei* on the domain Ω^k have the form

$$\boldsymbol{K}_{uu}^{k\tau s} = \int_{A_k} \big([-\boldsymbol{D}_p^\tau + \boldsymbol{A}_p^\tau]^T\ \boldsymbol{C}_{\sigma\epsilon}\ [\boldsymbol{D}_p^s + \boldsymbol{A}_p^s]\big)\boldsymbol{F}_\tau\boldsymbol{F}_s H_\alpha H_\beta\, dz,$$

$$\boldsymbol{K}_{u\sigma}^{k\tau s} = \int_{A_k} \big([\boldsymbol{D}_{nz}^\tau - \boldsymbol{A}_n^\tau - \boldsymbol{D}_{n\Omega}^\tau]^T + [-\boldsymbol{D}_p^\tau + \boldsymbol{A}_p^\tau]^T\boldsymbol{C}_{\sigma\sigma}\big)\boldsymbol{F}_\tau\boldsymbol{F}_s H_\alpha H_\beta\, dz,$$

$$\boldsymbol{K}_{ue}^{k\tau s} = \int_{A_k} \big(-[-\boldsymbol{D}_p^\tau + \boldsymbol{A}_p^\tau]^T\boldsymbol{C}_{\sigma\mathscr{E}}\boldsymbol{D}_{e\Omega}^s\big)\boldsymbol{F}_\tau\boldsymbol{F}_s H_\alpha H_\beta\, dz,$$

$$\boldsymbol{K}_{u\mathscr{D}}^{k\tau s} = \int_{A_k} \big([-\boldsymbol{D}_p^\tau + \boldsymbol{A}_p^\tau]^T\boldsymbol{C}_{\sigma\mathscr{D}}\big)\boldsymbol{F}_\tau\boldsymbol{F}_s H_\alpha H_\beta\, dz,$$

$$\boldsymbol{K}_{\sigma u}^{k\tau s} = \int_{A_k} \big((\boldsymbol{D}_{nz}^s + \boldsymbol{D}_{n\Omega}^s - \boldsymbol{A}_n^s) - \boldsymbol{C}_{\epsilon\epsilon}(\boldsymbol{D}_p^s + \boldsymbol{A}_p^s)\big)\boldsymbol{F}_\tau\boldsymbol{F}_s H_\alpha H_\beta\, dz,$$

$$\boldsymbol{K}_{\sigma\sigma}^{k\tau s} = \int_{A_k} -\boldsymbol{C}_{\epsilon\sigma}\boldsymbol{F}_\tau\boldsymbol{F}_s H_\alpha H_\beta\, dz,$$

$$\boldsymbol{K}_{\sigma e}^{k\tau s} = \int_{A_k} \boldsymbol{C}_{\epsilon\mathscr{E}}\boldsymbol{D}_{e\Omega}^s\boldsymbol{F}_\tau\boldsymbol{F}_s H_\alpha H_\beta\, dz, \qquad \boldsymbol{K}_{\sigma\mathscr{D}}^{k\tau s} = \int_{A_k} -\boldsymbol{C}_{\epsilon\mathscr{D}}\boldsymbol{F}_\tau\boldsymbol{F}_s H_\alpha H_\beta\, dz,$$

$$\boldsymbol{K}_{eu}^{k\tau s} = \int_{A_k} -\boldsymbol{D}_{e\Omega}^{\tau\,T}\boldsymbol{C}_{\mathscr{D}\epsilon}(\boldsymbol{D}_p^s + \boldsymbol{A}_p^s)\boldsymbol{F}_\tau\boldsymbol{F}_s H_\alpha H_\beta\, dz, \qquad \boldsymbol{K}_{e\sigma}^{k\tau s} = \int_{A_k} -\boldsymbol{D}_{e\Omega}^{\tau\,T}\boldsymbol{C}_{\mathscr{D}\sigma}\boldsymbol{F}_\tau\boldsymbol{F}_s H_\alpha H_\beta\, dz,$$

$$\boldsymbol{K}_{ee}^{k\tau s} = \int_{A_k} \boldsymbol{D}_{e\Omega}^{\tau\,T}\boldsymbol{C}_{\mathscr{D}\mathscr{E}}\boldsymbol{D}_{e\Omega}^s\boldsymbol{F}_\tau\boldsymbol{F}_s H_\alpha H_\beta\, dz, \qquad \boldsymbol{K}_{e\mathscr{D}}^{k\tau s} = \int_{A_k} (\boldsymbol{D}_{en}^{\tau\,T} - \boldsymbol{D}_{e\Omega}^{\tau\,T}\boldsymbol{C}_{\mathscr{D}\mathscr{D}})\boldsymbol{F}_\tau\boldsymbol{F}_s H_\alpha H_\beta\, dz,$$

$$\boldsymbol{K}_{\mathscr{D}u}^{k\tau s} = \int_{A_k} \boldsymbol{C}_{\mathscr{E}\epsilon}(\boldsymbol{D}_p^s + \boldsymbol{A}_p^s)\boldsymbol{F}_\tau\boldsymbol{F}_s H_\alpha H_\beta\, dz, \qquad \boldsymbol{K}_{\mathscr{D}\sigma}^{k\tau s} = \int_{A_k} \boldsymbol{C}_{\mathscr{E}\sigma}\boldsymbol{F}_\tau\boldsymbol{F}_s H_\alpha H_\beta\, dz,$$

$$\boldsymbol{K}_{\mathscr{D}e}^{k\tau s} = \int_{A_k} (\boldsymbol{D}_{en}^s - \boldsymbol{D}_{e\Omega}^s\boldsymbol{C}_{\mathscr{E}\mathscr{E}})\boldsymbol{F}_\tau\boldsymbol{F}_s H_\alpha H_\beta\, dz, \qquad \boldsymbol{K}_{\mathscr{D}\mathscr{D}}^{k\tau s} = \int_{A_k} \boldsymbol{C}_{\mathscr{E}\mathscr{D}}\boldsymbol{F}_\tau\boldsymbol{F}_s H_\alpha H_\beta\, dz.$$

The *fundamental nuclei* on the boundary Γ^k are

$$\boldsymbol{\Pi}_{uu}^{k\tau s} = \int_{A_k} \boldsymbol{I}_p^T \boldsymbol{C}_{\sigma\epsilon}(\boldsymbol{D}_p^s + \boldsymbol{A}_p^s)\boldsymbol{F}_\tau \boldsymbol{F}_s H_\alpha H_\beta \, dz, \qquad \boldsymbol{\Pi}_{eu}^{k\tau s} = \int_{A_k} \boldsymbol{I}_{e\Omega}^T \boldsymbol{C}_{\mathscr{D}\epsilon}(\boldsymbol{D}_p^s + \boldsymbol{A}_p^s)\boldsymbol{F}_\tau \boldsymbol{F}_s H_\alpha H_\beta \, dz,$$

$$\boldsymbol{\Pi}_{u\sigma}^{k\tau s} = \int_{A_k} (\boldsymbol{I}_{n\Omega}^T + \boldsymbol{I}_p^T \boldsymbol{C}_{\sigma\sigma})\boldsymbol{F}_\tau \boldsymbol{F}_s H_\alpha H_\beta \, dz, \qquad \boldsymbol{\Pi}_{e\sigma}^{k\tau s} = \int_{A_k} \boldsymbol{I}_{e\Omega}^T \boldsymbol{C}_{\mathscr{D}\sigma} \boldsymbol{F}_\tau \boldsymbol{F}_s H_\alpha H_\beta \, dz,$$

$$\boldsymbol{\Pi}_{ue}^{k\tau s} = \int_{A_k} -(\boldsymbol{I}_p^T \boldsymbol{C}_{\sigma\mathscr{E}} \boldsymbol{D}_{e\Omega}^s)\boldsymbol{F}_\tau \boldsymbol{F}_s H_\alpha H_\beta \, dz, \qquad \boldsymbol{\Pi}_{ee}^{k\tau s} = \int_{A_k} -\boldsymbol{I}_{e\Omega}^T \boldsymbol{C}_{\mathscr{D}\mathscr{E}} \boldsymbol{D}_{e\Omega}^s \boldsymbol{F}_\tau \boldsymbol{F}_s H_\alpha H_\beta \, dz,$$

$$\boldsymbol{\Pi}_{u\mathscr{D}}^{k\tau s} = \int_{A_k} \boldsymbol{I}_p^T \boldsymbol{C}_{\sigma\mathscr{D}} \boldsymbol{F}_\tau \boldsymbol{F}_s H_\alpha H_\beta \, dz, \qquad \boldsymbol{\Pi}_{e\mathscr{D}}^{k\tau s} = \int_{A_k} \boldsymbol{I}_{e\Omega}^T \boldsymbol{C}_{\mathscr{D}\mathscr{D}} \boldsymbol{F}_\tau \boldsymbol{F}_s H_\alpha H_\beta \, dz,$$

where some auxiliary arrays have been introduced to facilitate integration by parts:

$$\boldsymbol{I}_p = \begin{bmatrix} 1/H_\alpha & 0 & 0 \\ 0 & 1/H_\beta & 0 \\ 1/H_\beta & 1/H_\alpha & 0 \end{bmatrix}, \quad \boldsymbol{I}_{n\Omega} = \begin{bmatrix} 0 & 0 & 1/H_\alpha \\ 0 & 0 & 1/H_\beta \\ 0 & 0 & 0 \end{bmatrix}, \quad \boldsymbol{I}_{e\Omega} = \begin{bmatrix} 1/H_\alpha & 0 & 0 \\ 0 & 1/H_\beta & 0 \\ 0 & 0 & 0 \end{bmatrix}. \tag{24}$$

Closed-form solutions. Navier-type closed-form solutions are possible for the governing equations derived in the previous section if the materials are *transversely isotropic*, that is, if they fulfill the conditions

$$C_{pp16} = C_{pp26} = C_{pn63} = C_{pn36} = C_{nn45} = 0, \quad e_{25} = e_{14} = e_{36} = 0, \quad \varepsilon_{12}^\epsilon = \varepsilon_{21}^\epsilon = 0. \tag{25}$$

The following harmonic assumptions can be made for the field variables:

$$\begin{aligned} (u_{\alpha_\tau}^k, \sigma_{\alpha z_\tau}^k) &= \sum_{m,n} (U_{\alpha_\tau}^k, S_{\alpha z_\tau}^k) \cos\frac{m\pi\alpha_k}{a_k} \sin\frac{n\pi\beta_k}{b_k}, & k = 1, N_l, \\ (u_{\beta_\tau}^k, \sigma_{\beta z_\tau}^k) &= \sum_{m,n} (U_{\beta_\tau}^k, S_{\beta z_\tau}^k) \sin\frac{m\pi\alpha_k}{a_k} \cos\frac{n\pi\beta_k}{b_k}, & \tau = t, b, r, \\ (u_{z_\tau}^k, \sigma_{zz_\tau}^k, p_{z_\tau}^k, \Phi_\tau^k, \mathscr{D}_{n_\tau}^k) &= \sum_{m,n} (U_{z_\tau}^k, S_{zz_\tau}^k, P_{z_\tau}^k, \hat{\Phi}_\tau^k, \hat{\mathscr{D}}_{n_\tau}^k) \sin\frac{m\pi\alpha_k}{a_k} \sin\frac{n\pi\beta_k}{b_k}, & r = 2, N, \end{aligned} \tag{26}$$

in which a_k and b_k are the shell lengths in the α_k and β_k directions, and m and n are the correspondent wave numbers. These assumptions correspond to simply supported boundary conditions.

Upon substitution of Equation (26), the governing equations on Ω^k assume the form of a linear system of algebraic equations in the domain while the boundary conditions are exactly fulfilled.

The final form of that system of algebraic equations at the multilayer shell level could be formally written as follows:

$$\begin{aligned} \hat{\boldsymbol{K}}_{uu}\hat{\boldsymbol{u}} + \hat{\boldsymbol{K}}_{u\sigma}\hat{\boldsymbol{\sigma}}_{\boldsymbol{n}} + \hat{\boldsymbol{K}}_{ue}\hat{\boldsymbol{\Phi}} + \hat{\boldsymbol{K}}_{u\mathscr{D}}\hat{\mathscr{D}}_{\boldsymbol{n}} &= \boldsymbol{p}, \\ \hat{\boldsymbol{K}}_{\sigma u}\hat{\boldsymbol{u}} + \hat{\boldsymbol{K}}_{\sigma\sigma}\hat{\boldsymbol{\sigma}}_{\boldsymbol{n}} + \hat{\boldsymbol{K}}_{\sigma e}\hat{\boldsymbol{\Phi}} + \hat{\boldsymbol{K}}_{\sigma\mathscr{D}}\hat{\mathscr{D}}_{\boldsymbol{n}} &= 0, \\ \hat{\boldsymbol{K}}_{eu}\hat{\boldsymbol{u}} + \hat{\boldsymbol{K}}_{e\sigma}\hat{\boldsymbol{\sigma}}_{\boldsymbol{n}} + \hat{\boldsymbol{K}}_{ee}\hat{\boldsymbol{\Phi}} + \hat{\boldsymbol{K}}_{e\mathscr{D}}\hat{\mathscr{D}}_{\boldsymbol{n}} &= \boldsymbol{p_e}, \\ \hat{\boldsymbol{K}}_{\mathscr{D}u}\hat{\boldsymbol{u}} + \hat{\boldsymbol{K}}_{\mathscr{D}\sigma}\hat{\boldsymbol{\sigma}}_{\boldsymbol{n}} + \hat{\boldsymbol{K}}_{\mathscr{D}e}\hat{\boldsymbol{\Phi}} + \hat{\boldsymbol{K}}_{\mathscr{D}\mathscr{D}}\hat{\mathscr{D}}_{\boldsymbol{n}} &= 0. \end{aligned} \tag{27}$$

An example of the explicit form of the fundamental nuclei for the k-layer is reported in the Appendix. The layer arrays are used to obtain multilayer matrices, using the assembly techniques described in [Carrera 2003].

8. Numerical results

This section discusses numerical computations for piezoelectric shells, comparing F-RMVT results with the P-RMVT and PVD results described in [Carrera and Brischetto 2007].

Acronyms of theories. Depending on the used variational statement (PVD or RMVT), variables description and order of expansion N, a number of two-dimensional shell theories can be derived. To identify the various theories, appropriate acronyms are introduced, built as shown in the chart. The first field can be E or L, denoting the ESL or LW description, respectively; the second field can be D, M or FM according to PVD, RMVT application and RMVT application with normal electric displacement modeled; the last field can take on the numbers 1–4 according to the order of the adopted expansion in the thickness direction; a third Z and fourth C field (optional in the ESL case) denote the use of MZZF and/or IC fulfillment, respectively. FSDT results are obtained as particular case of ED1 ones, while CLT solutions have been computed by application of a penalty technique to a shear correction factor of FSDT. Stiffness coefficients related to FSDT and CLT are those of three-dimensional Hooke's Law; that is, no plane stress problems have been imposed.

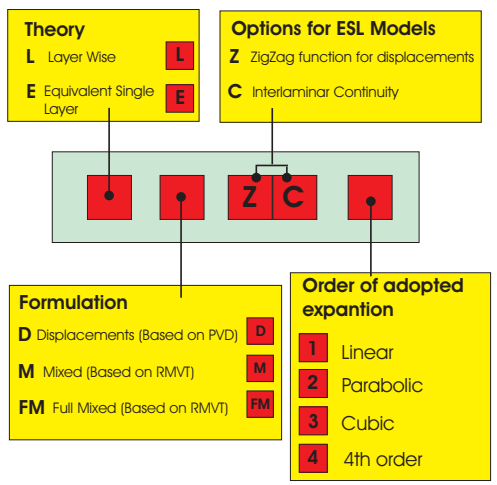

Preliminary assessment. The piezoelectric plates for which three-dimensional solutions were given in [Heyliger 1997] are considered. The two cases of a sensor (where a bisinusoidal distribution of mechanical pressure is applied) and an actuator (where a bisinusoidal distribution of electric voltage is applied) are considered in Figure 3, which also shows the Cartesian reference system used. The material properties are those in columns 1 and 2 of Table 1. A four-layer plate has been analyzed. The two external layers

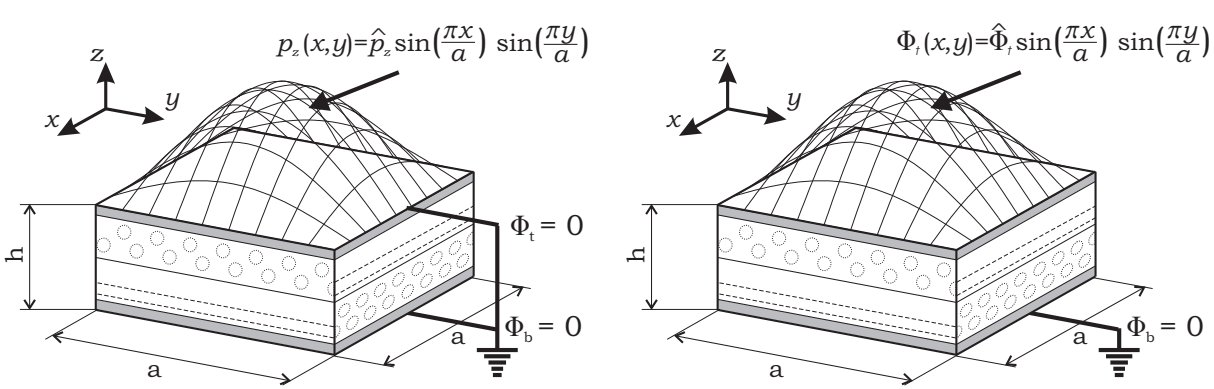

Figure 3. Geometry and boundary conditions for the sensor (left) and actuator (right) configurations.

	PZT-4	Gr/EP	PVDF [Dumir et al. 1997]	Piezo [Chen et al. 1996]	Composite
E_1 [GPa]	81.3	132.38	2	2	172
E_2 [GPa]	81.3	10.756	2	2	6.9
E_3 [GPa]	64.5	10.756	2	2	6.9
ν_{12} [−]	0.329	0.24	1/3	0.29	0.25
ν_{13} [−]	0.432	0.24	1/3	0.29	0.25
ν_{23} [−]	0.432	0.49	1/3	0.29	0.25
G_{23} [GPa]	25.6	3.606	0.75	0.7752	1.4
G_{13} [GPa]	25.6	5.6537	0.75	0.7752	3.4
G_{12} [GPa]	30.6	5.6537	0.75	0.7752	3.4
e_{15} [C/m^2]	12.72	0	0	0	0
e_{24} [C/m^2]	12.72	0	0	0	0
e_{31} [C/m^2]	−5.20	0	−0.0015	0.046	0
e_{32} [C/m^2]	−5.20	0	0.0285	0	0
e_{33} [C/m^2]	15.08	0	−0.051	0	0
$\varepsilon_{11}/\varepsilon_0$ [−]	1475	3.5	–	–	–
$\varepsilon_{22}/\varepsilon_0$ [−]	1475	3.0	–	–	–
$\varepsilon_{33}/\varepsilon_0$ [−]	1300	3.0	–	–	–
ε_{11} [pC/Vm]	1.306×10^4	–	106.2	106.0	13060
ε_{22} [pC/Vm]	1.306×10^4	–	106.2	106.0	13060
ε_{33} [pC/Vm]	1.151×10^4	–	106.2	106.0	13060

Table 1. Electromechanical properties of the materials considered.

are made of piezoelectric material and have thickness $h_e = 0.1h_{\text{tot}}$. The two internal layers are of a unidirectional composite with fiber orientation 0°/90° and thickness $h_i = 0.4h_{\text{tot}}$. Results for mechanical and electrical variables related to the sensor piezoelectric plates are given in Table 2, allowing further insight into the results already discussed in [Ballhause et al. 2004; D'Ottavio and Kröplin 2006; Carrera and Brischetto 2007]. The tables show the tranverse distribution of the transverse normal stress and the normal electric displacement for a thick plate geometry. Higher-order LW results related to P-RMVT, F-RMVT and PVD applications are compared to exact three-dimensional solutions. Mixed theories fulfilling C_z^0-requirements (partial and full) give better normal stress results with respect to classical theories (LD4 and LD3 do not fulfill the continuity of σ_{zz} through the interfaces). The best results for $\mathfrak{D}_z$ are obtained via F-RMVT analysis under the assumption of *a priori* electrical and mechanical interlaminar continuity; indeed, LFM4 and LFM3 allow one to assume continuous $\mathfrak{D}_z$ through the interfaces.

The actuator case is considered in Table 3, which shows the electric potential obtained from high-order expansions compared with those from a 3D solution. PVD, P-RMVT and F-RMVT, are all suitable for

z/h	3D	LD4	LM4	LFM4	LD3	LM3	LFM3
0.500	1.0000	1.0000	1.0001	1.0001	1.0013	0.9994	0.9994
0.400	0.9515	0.9515	0.9516	0.9516	0.9502	0.9522	0.9522
0.400	0.9515	0.9518	0.9516	0.9516	0.9611	0.9522	0.9522
0.300	0.8520	0.8517	0.8517	0.8517	0.8479	0.8515	0.8515
0.200	0.7375	0.7376	0.7375	0.7375	0.7376	0.7376	0.7376
0.100	0.6169	0.6168	0.6169	0.6169	0.6207	0.6171	0.6171
0.000	0.4983	0.4986	0.4984	0.4984	0.4888	0.4977	0.4977
0.000	0.4983	0.4982	0.4984	0.4984	0.5067	0.4977	0.4977
−0.100	0.3805	0.3805	0.3804	0.3804	0.3771	0.3807	0.3807
−0.200	0.2614	0.2613	0.2614	0.2614	0.2613	0.2613	0.2613
−0.300	0.1482	0.1485	0.1484	0.1485	0.1518	0.1482	0.1482
−0.400	0.0487	0.0485	0.0487	0.0487	0.0403	0.0492	0.0492
−0.400	0.0487	0.0487	0.0487	0.0487	0.0499	0.0492	0.0492
−0.500	0.0000	0.0000	0.0000	0.0000	−0.0012	−0.0006	−0.0006
0.500	160.58	160.58	160.61	160.51	161.18	160.14	160.93
0.400	−0.3382	−0.3348	−0.4734	−0.3383	−0.9356	−4.1211	−0.3380
0.400	−0.3382	−0.3384	−0.3384	−0.3383	−0.3369	−0.3369	−0.3380
0.300	−0.1276	−0.1277	−0.1277	−0.1277	−0.1283	−0.1283	−0.1278
0.200	0.0813	0.0813	0.0813	0.0813	0.0813	0.0813	0.0813
0.100	0.2913	0.2914	0.2914	0.2914	0.2920	0.2920	0.2916
0.000	0.5052	0.5053	0.5053	0.5053	0.5038	0.5038	0.5050
0.000	0.5052	0.5053	0.5053	0.5053	0.5070	0.5070	0.5050
−0.100	0.7259	0.7262	0.7262	0.7262	0.7256	0.7256	0.7264
−0.200	0.9563	0.9565	0.9565	0.9565	0.9565	0.9565	0.9565
−0.300	1.1995	1.2000	1.2000	1.2000	1.2007	1.2007	1.1999
−0.400	1.4587	1.4590	1.4590	1.4590	1.4573	1.4573	1.4593
−0.400	1.4587	1.4559	1.3599	1.4590	1.9984	2.9753	1.4593
−0.500	−142.46	−142.46	−142.43	−142.39	−143.00	−142.69	−142.77

Table 2. Through the thickness distribution of (top) transverse normal stress σ_{zz} and (bottom) normal electric displacement $\mathcal{D}_z$ in 10^{13}, for the sensor case, with $a/h = 4$. Comparison of various approaches versus 3D solution.

this case; the electric potential is, in fact, a primary variable for all three models. The main advantage of F-RMVT with respect to P-RMVT is the fulfillment of C_z^0-requirements for normal electric displacement.

Further evaluation of the proposed model can be gleaned from the next few tables. A shell problem proposed in [Chen et al. 1996] is considered in Table 4, where 3D solutions are compared with respect to PVD, P-RMVT and F-RMVT models; mechanical displacements at middle surface are considered. This problem refers to a Ren shell [1987] with three mechanical cross-ply layers (90°/0°/90°) and two external piezoelectric layers (see fifth and fourth columns of Table 1). The thickness of each piezoelectric layer

z/h	3D	LD4	LM4	LFM4	LD3	LM3	LFM3
0.500	1.0000	1.0000	1.0000	1.0000	1.0000	1.0000	1.0000
0.400	0.9929	0.9929	0.9929	0.9929	0.9929	0.9929	0.9929
0.400	0.9929	0.9929	0.9929	0.9929	0.9929	0.9929	0.9929
0.300	0.8415	0.8418	0.8418	0.8418	0.8418	0.8418	0.8418
0.200	0.7014	0.7015	0.7015	0.7015	0.7014	0.7014	0.7014
0.100	0.5707	0.5709	0.5709	0.5709	0.5709	0.5709	0.5709
0.000	0.4476	0.4477	0.4477	0.4477	0.4477	0.4477	0.4476
0.000	0.4476	0.4477	0.4477	0.4477	0.4477	0.4477	0.4476
−0.100	0.3305	0.3307	0.3307	0.3307	0.3307	0.3307	0.3307
−0.200	0.2179	0.2179	0.2179	0.2179	0.2179	0.2179	0.2179
−0.300	0.1081	0.1082	0.1082	0.1082	0.1082	0.1082	0.1082
−0.400	−0.0010	−0.0010	−0.0010	−0.0010	−0.0010	−0.0010	−0.0010
−0.400	−0.0010	−0.0010	−0.0010	−0.0010	−0.0010	−0.0010	−0.0010
−0.500	0.0000	0.0000	0.0000	0.0000	0.0000	0.0000	0.0000

Table 3. Through the thickness distribution of electric potential Φ for the actuator case, with $a/h = 4$. Comparison of various approaches versus 3D solution.

R_β/h_c	2	4	10	50	100	2	4	10	50	100
	$\bar{u}_z$ $(z=0)$					$\bar{u}_\beta$ $(z=0)$				
Ref	1.440	0.459	0.144	0.0808	0.0785	5.294	1.549	0.480	0.269	0.262
LM4	1.443	0.458	0.144	0.0810	0.0787	5.308	1.547	0.479	0.270	0.262
LD4	1.443	0.458	0.144	0.0810	0.0787	5.305	1.547	0.479	0.270	0.262
LFM4	1.443	0.458	0.144	0.0810	0.0787	5.308	1.549	0.479	0.270	0.262
LM3	1.442	0.458	0.144	0.0810	0.0787	5.306	1.547	0.479	0.270	0.262
LD3	1.442	0.458	0.144	0.0810	0.0787	5.299	1.547	0.479	0.270	0.262
LFM3	1.442	0.458	0.144	0.0810	0.0787	5.306	1.547	0.479	0.270	0.262

Table 4. Mechanical displacements for a five-layer piezomechanic Ren shell [Chen et al. 1996]; the numbers given are $\bar{u}_z = 10\, E_3\, u_z\, h_c^3/(P_z R_\beta^4)$ and $\bar{u}_\beta = 100\, E_3\, u_\beta\, h_c^3/P_z R_\beta^4$. Comparison with exact 3D solution.

is one hundredth of the total ($h_p = 1/100\, h_c$). Loading conditions are: $\Phi_t = \Phi_b = 0$ and $P_z = 1$ at top. F-RMVT results are very similar to 3D solutions and to PVD and P-RMVT models: the piezoelectric layers are, in fact, very thin and mechanical displacements are the primary variables in the three proposed variational statements.

Table 5 shows a comparison of the results obtained with the present models with the three-dimensional solution from [Dumir et al. 1997] for a one-layer piezoelectric Ren shell, whose material properties are reported in column 3 of Table 1. The loading conditions are $\Phi_t = \Phi_b = 0$ and $P_z = 1$ at the top. F-RMVT

R_β/h	Ref	LM4	LM3	LFM4	LFM3
		$\overline{w}\ (z=-h/2)$			
2	−28.65	−28.63	−28.46	−28.63	−28.46
4	−20.55	−20.55	−20.54	−20.55	−20.54
6	⟵ −18.72 ⟶		**10**	⟵ −17.60 ⟶	
20	−16.96	−16.95	−16.95	−16.95	−16.95
100	⟵ −16.55 ⟶		**500**	⟵ −16.48 ⟶	
		$\overline{w}\ (z=0)$			
2	−31.47	−31.45	−31.41	−31.45	−31.41
4	⟵ −21.10 ⟶		**6**	⟵ −18.96 ⟶	
10	⟵ −17.68 ⟶		**20**	⟵ −16.98 ⟶	
100	⟵ −16.55 ⟶		**500**	⟵ −16.48 ⟶	
		$\overline{w}\ (z=h/2)$			
2	−31.31	−31.30	−31.14	−31.30	−31.14
4	−20.65	−20.65	−20.64	−20.65	−20.64
6	⟵ −18.73 ⟶				
10	⟵ −17.60 ⟶		**20**	⟵ −16.95 ⟶	
100	⟵ −16.55 ⟶		**500**	⟵ −16.48 ⟶	
		$\overline{v}\ (z=-h/2)$			
2	−23.61	−23.59	−23.38	−23.59	−23.38
4	−13.09	−13.09	−13.08	−13.09	−13.08
6	−10.23	−10.23	−10.22	−10.22	−10.22
10	⟵ −8.177 ⟶		**20**	⟵ −6.778 ⟶	
100	⟵ −5.738 ⟶		**500**	⟵ −5.539 ⟶	
		$\overline{v}\ (z=h/2)$			
2	2.046	2.045	2.029	2.045	2.029
4	−0.8806	−0.8806	−0.8799	−0.8806	−0.8799
6	−2.331	−2.331	−2.330	−2.331	−2.330
10	⟵ −3.572 ⟶				
20	−4.528	−4.528	−4.527	−4.527	−4.527
100	⟵ −5.297 ⟶		**500**	⟵ −5.451 ⟶	
		$\overline{\sigma}_{zz}\ (z=0)$			
2	−0.2906	−0.2359	−0.2922	−0.2359	−0.2922
4	0.2170	0.2453	0.2181	0.2453	0.2181
6	0.6356	0.6541	0.6365	0.6541	0.6365
10	1.420	1.430	1.420	1.430	1.420
20	3.319	3.325	3.320	3.325	3.320
100	⟵ 18.34 ⟶		**500**	⟵ 93.34 ⟶	

R_β/h	Ref	LM4	LM3	LFM4	LFM3
		$\overline{\sigma}_{\beta z}\ (z=0)$			
2	−0.6653	−0.6742	−0.6706	−0.6742	−0.6706
4	−0.6238	−0.6261	−0.6252	−0.6261	−0.6252
6	−0.6055	−0.6065	−0.6061	−0.6065	−0.6061
10	−0.5893	−0.5896	−0.5895	−0.5896	−0.5895
20	−0.5762	−0.5763	−0.5763	−0.5763	−0.5763
100	⟵ −0.5653 ⟶		**500**	⟵ −0.5631 ⟶	
		$10^3\overline{\Phi}\ (z=0)$			
2	1.734	1.729	1.847	1.729	1.847
4	2.443	2.442	2.477	2.442	2.477
6	2.541	2.540	2.556	2.540	2.556
10	2.560	2.560	2.565	2.560	2.565
20	2.540	2.540	2.541	2.540	2.541
100	⟵ 2.504 ⟶		**500**	⟵ 2.494 ⟶	
		$10\overline{\mathcal{D}}_z\ (z=-h/2)$			
2	5.908	−9.206	−10.27	6.381	7.326
4	2.550	−16.26	−16.92	2.670	3.299
6	1.532	−31.74	−32.19	1.584	2.017
10	0.7830	−82.68	−82.94	0.8008	1.0622
20	0.2659	−320.7	−320.9	0.2702	0.4003
100	−0.1171	−7861	−7861	−0.1169	−0.0911
500	−0.1902	−195747	−195747	−0.1902	−0.1851
		$10\overline{\mathcal{D}}_z\ (z=h/2)$			
2	0.8480	−5.641	−4.502	1.1484	−0.1072
4	0.0213	−14.28	−13.62	0.1161	−0.5774
6	−0.0996	−30.43	−29.98	−0.0557	−0.5155
10	−0.1575	−81.90	−81.64	−0.1413	−0.4121
20	−0.1860	−320.4	−320.3	−0.1820	−0.3143
100	−0.2041	−7861	−7861	−0.2039	−0.2298
500	−0.2075	−195747	−195747	−0.2075	−0.2126
		$10\overline{\mathcal{D}}_\beta\ (z=0)$			
2	−0.3070	−0.3060	−0.3270	−0.3060	−0.3270
4	−0.4324	−0.4323	−0.4384	−0.4323	−0.4384
6	−0.4497	−0.4497	−0.4524	−0.4497	−0.4524
10	−0.4531	−0.4531	−0.4541	−0.4531	−0.4541
20	−0.4496	−0.4496	−0.4498	−0.4496	−0.4498
100	⟵ −0.4431 ⟶				
500	−0.4415	−0.4415	−0.4414	−0.4414	−0.4414

Table 5. One-layer piezoelectric Ren shell: present analysis vs. exact solutions [Dumir et al. 1997]. Values of $R\beta/h$ in bold; $\leftarrow x \rightarrow$ indicates that all 5 row values equal x.

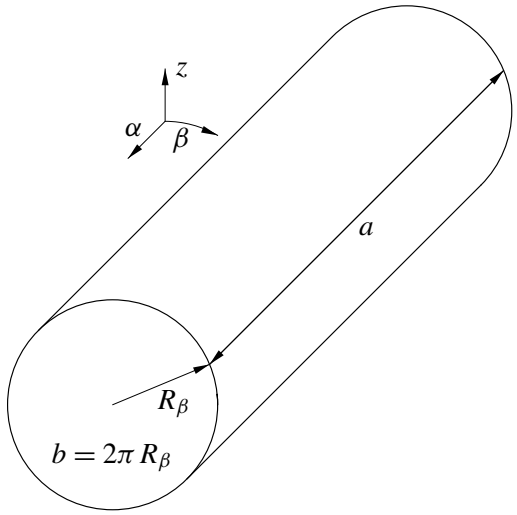

Figure 4. Proposed benchmark: cylindrical shell, geometry and notation from [Varadan and Bhaskar 1991].

and P-RMVT models are compared to exact solutions for different values of the thickness ratio. This table confirms the validity of F-RMVT model: the limitations for $\mathfrak{D}_z$ evaluation exhibited by P-RMVT model (see also [Carrera and Brischetto 2007]) have been overcome by F-RMVT.

Proposed benchmarks. In this section the shell problems for which 3D solution were given in [Varadan and Bhaskar 1991] for the pure mechanical problem are extended to the piezoelectric case. The problem was studied in [Carrera 1999a; 1999b] to assess the Unified Formulation in both PVD and RMVT for pure mechanical problems. The piezoelectric shells considered here are built by replacing and/or adding piezoelectric layers to the original shells. The material properties of these layers coincide with those already used for the piezoelectric plates.

The cylindrical shell considered by Bhaskar and Varadan has the geometric parameters $a = 40$, $b = 20\pi$, $R_\alpha = \infty$, $R_\beta = 10$, $m = 1$, $n = 8$; see Figure 4.

Two layouts are considered: one piezoelectric layer, and then four layers, the two external layers being made of piezoelectric material, and the two internal ones of carbon fiber cross-ply (0°/90°). The mechanical and geometrical properties are those used in the plate case. Both actuator and sensor configurations are treated. For the actuator case the distribution of electric potential Φ applied at top surface is

$$\Phi(\alpha, \beta) = \overline{\Phi} \sin \frac{\pi\alpha}{a} \sin \frac{8\pi\beta}{b}, \tag{28}$$

with $\overline{\Phi}_t = 1$, $\overline{\Phi}_b = 0$ and $\overline{P}_z = 0$.

Transverse mechanical pressure is applied at the bottom surface in the sensor case:

$$P_z(\alpha, \beta) = \overline{P}_z \sin \frac{\pi\alpha}{a} \sin \frac{8\pi\beta}{b}, \tag{29}$$

with $\overline{\Phi}_{top} = \overline{\Phi}_b = 0$, and $\overline{P}_z = 1$.

Results are given in the next few tables and figures, which compare different variational treatments for thick and thin shells, showing the electric potential, normal electric displacement, transverse displacement $w \equiv u_z$, and normal stress σ_{zz}. Table 6, left, referring to the one-layer actuator case, shows that higher-order expansions leads to the same results for both electric potential and mechanical displacement,

R_β/h	2	4	10	100	R_β/h	2	4	10	100
		Φ $(z=0)$					Φ $(z=0)$		
LD4	0.3431	0.4611	0.5037	0.5254	LD4	0.0153	0.0355	0.0942	0.6513
LM1	0.5000	0.5000	0.5000	0.5000	LM1	0.0000	0.0000	0.0000	0.0000
LM4	0.3431	0.4611	0.5037	0.5254	LM4	0.0153	0.0355	0.0942	0.6513
LFM1	0.5000	0.5000	0.5000	0.5000	LFM1	0.0000	0.0000	0.0000	0.0000
LFM2	0.3415	0.4609	0.5037	0.5254	LFM2	0.0150	0.0350	0.0939	0.6513
LFM3	0.3436	0.4614	0.5037	0.5254	LFM3	0.0161	0.0359	0.0943	0.6514
LFM4	0.3431	0.4611	0.5037	0.5254	LFM4	0.0153	0.0355	0.0942	0.6513
		$\mathcal{D}_z 10^{11}$ $(z=h/2)$					$\mathcal{D}_z 10^{9}$ $(z=h/2)$		
LD4	−605.73	−801.76	−1622.9	−10416	LD4	0.0224	0.1377	2.0958	1456.1
LM1	−350.00	−662.37	−1608.6	−11711	LM1	−0.1144	−0.2121	0.1311	1118.0
LM4	−605.73	−801.76	−1622.9	−10416	LM4	0.0224	0.1377	2.0958	1456.1
LFM1	−327.37	−642.20	−1599.7	−16656	LFM1	−0.1340	−0.3506	−1.7252	−197.53
LFM2	−529.21	−743.93	−1593.3	−16262	LFM2	0.0407	0.0378	−0.0937	−111.27
LFM3	−587.25	−787.72	−1616.7	−16266	LFM3	0.0045	0.0092	−0.1536	−111.76
LFM4	−584.80	−783.99	−1615.6	−16266	LFM4	0.0095	0.0028	−0.1646	−111.76
		$W 10^{11}$ $(z=0)$					$W 10^{9}$ $(z=0)$		
LD4	−9.6220	−11.285	6.4540	11277	LD4	0.0566	0.3332	4.5483	3016.6
LM1	−21.851	−18.528	2.9362	9531.4	LM1	0.0623	0.2956	3.6212	2530.3
LM4	−9.6220	−11.285	6.4540	11277	LM4	0.0566	0.3332	4.5483	3016.6
LFM1	−21.850	−18.528	2.9353	9531.4	LFM1	0.0623	0.2955	3.6210	2530.3
LFM2	−9.4240	−11.030	6.5318	11276	LFM2	0.0530	0.3223	4.5169	3016.5
LFM3	−9.6061	−11.282	6.4540	11277	LFM3	0.0566	0.3331	4.5482	3016.6
LFM4	−9.6220	−11.285	6.4540	11277	LFM4	0.0566	0.3332	4.5483	3016.6
		σ_{zz} $(z=h/2)$					σ_{zz} $(z=-h/2)$		
LD4	3.0350	2.5512	1.0498	−836.32	LD4	−1.5105	−3.0742	−33.331	−22413
LM1	−0.4037	−0.1264	0.6259	54.231	LM1	−1.0564	−3.6212	−20.878	−1473.3
LM4	0.0431	0.0114	0.0004	−0.0001	LM4	−1.1392	−1.0671	−1.0269	−1.0018
LFM1	−0.4037	−0.1264	0.6258	54.231	LFM1	−1.0551	−3.6198	−20.877	−1473.3
LFM2	0.4285	0.4332	0.1982	−0.3861	LFM2	−1.1380	−1.5644	−2.6532	−12.288
LFM3	−0.0260	−0.0347	0.0005	0.0098	LFM3	−1.3463	−1.3907	−1.4043	−1.2716
LFM4	0.0431	0.0114	0.0004	−0.0001	LFM4	−1.1392	−1.0671	−1.0269	−1.0018

Table 6. Proposed benchmark: one-layer piezoelectric shell in the Varadan–Bhaskar geometry (Figure 4). Comparison of approaches. Left, actuator case; right, sensor case.

regardless of variational statement. Normal stress fulfills the boundary conditions at the top ($\sigma_{zz} = 0$ at the top for actuator case) in the case of P-RMVT and F-RMVT; however higher-order expansions are required. Normal electric displacement results related to F-RMVT applications are quite different with respect to PVD and P-RMVT ones (where $\mathcal{D}_z$ is not an assumed variable). These differences are larger for the sensor case, as will be seen.

Table 6, right, refers to the sensor case. The same comments for the left half of the table are made for electric potential, mechanical displacement and normal stress evaluation. Mechanical loading is applied at the bottom of the shell; such a boundary condition is exactly fulfilled by P-RMVT and F-RMVT applications. F-RMVT is more effective with respect to the other models for normal electric displacement evaluations.

The comments made in connection with Table 6 are confirmed for Table 7, which refers to a four-layer configuration. The differences in the evaluation of $\mathcal{D}_z$ are, in fact, larger for the sensor case. The presence of two mechanical layers reduces the electric coupling. Furthermore, for the sensor case the effect of the radii of curvature is larger than in the actuator case. The fulfillment of boundary conditions for transverse normal stress at the shell bottom demands the use of higher-order expansions and mixed theories; this is confirmed by an analysis of Table 7 (in contrast, higher-order PVD theories leads to an accurate evaluation of σ_{zz} in the case of a plate. This is not so in the shell case because of the curvature).

Figure 5 shows that discrepancies for $\mathcal{D}_z$ among F-RMVT, P-RMVT and PVD increase in the sensor case. Figure 6 refers to a multilayer shell: the capability of F-RMVT analysis to fulfill the interlaminar continuity of $\mathcal{D}_z$ is clearly shown. Transverse normal stress evaluation is given in Figure 7. The superiority of F-RMVT and P-RMVT with respect to PVD is confirmed.

Appendix: Explicit forms of fundamental nuclei

We detail here the algebraic forms related to closed-form solution for the nuclei $\boldsymbol{K}_{u\mathcal{D}}^{k\tau s}$:

$$(K_{u\mathcal{D}})_{11} = \frac{\alpha J_\beta^{k\tau s}(C_{nn33}e_{31} - C_{pn13}e_{33})}{e_{33}^2 + C_{nn33}\varepsilon_{33}}, \qquad (K_{u\mathcal{D}})_{12} = 0, \qquad (K_{u\mathcal{D}})_{13} = 0,$$

$$(K_{u\mathcal{D}})_{21} = \frac{\beta J_\alpha^{k\tau s}(C_{nn33}e_{32} - C_{pn23}e_{33})}{e_{33}^2 + C_{nn33}\varepsilon_{33}}, \qquad (K_{u\mathcal{D}})_{22} = 0, \qquad (K_{u\mathcal{D}})_{23} = 0,$$

$$(K_{u\mathcal{D}})_{31} = \frac{-C_{nn33}e_{31}\dfrac{\lambda_D}{R_\alpha}J_\beta^{k\tau s} - C_{nn33}e_{32}\dfrac{\lambda_D}{R_\beta}J_\alpha^{k\tau s} + C_{pn13}e_{33}\dfrac{\lambda_D}{R_\alpha}J_\beta^{k\tau s} + C_{pn23}e_{33}\dfrac{\lambda_D}{R_\beta}J_\alpha^{k\tau s}}{e_{33}^2 + C_{nn33}\varepsilon_{33}},$$

$$(K_{u\mathcal{D}})_{32} = 0, \qquad (K_{u\mathcal{D}})_{33} = 0,$$

where we have introduced the integrals

$$J_\alpha^{k\tau s} = \int_{h_k} F_\tau F_s H_\alpha \, dz, \qquad J_\beta^{k\tau s} = \int_{h_k} F_\tau F_s H_\beta \, dz. \tag{30}$$

The particular case of flat plates can be easily obtained by taking $R_\alpha^k = R_\beta^k = \infty$.

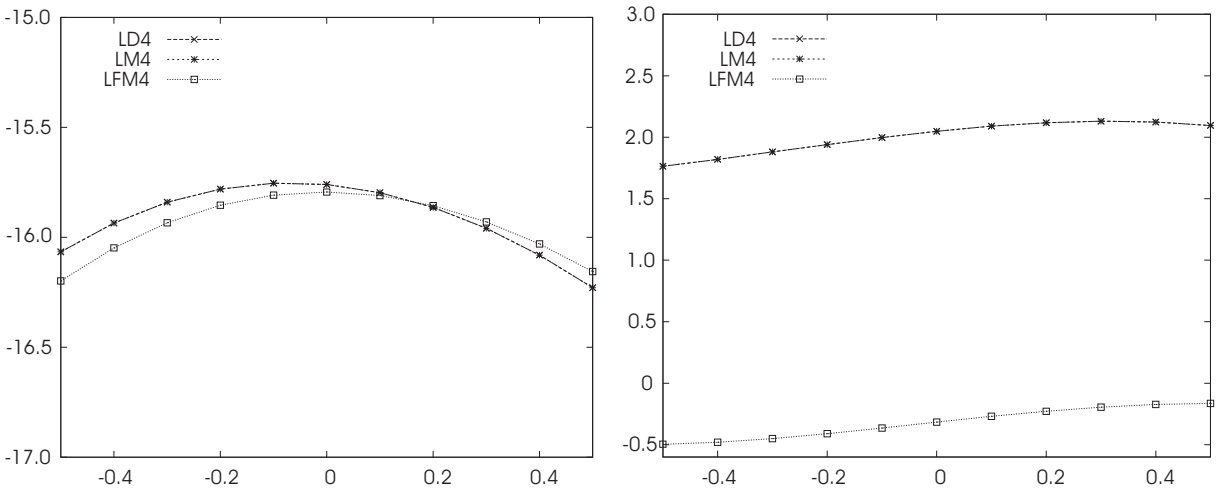

Figure 5. Proposed benchmark: plot of $\mathcal{D}_z 10^9$ versus z for one-layer piezoelectric shell, with $R_\beta/h = 10$. Left, actuator case; right, sensor case.

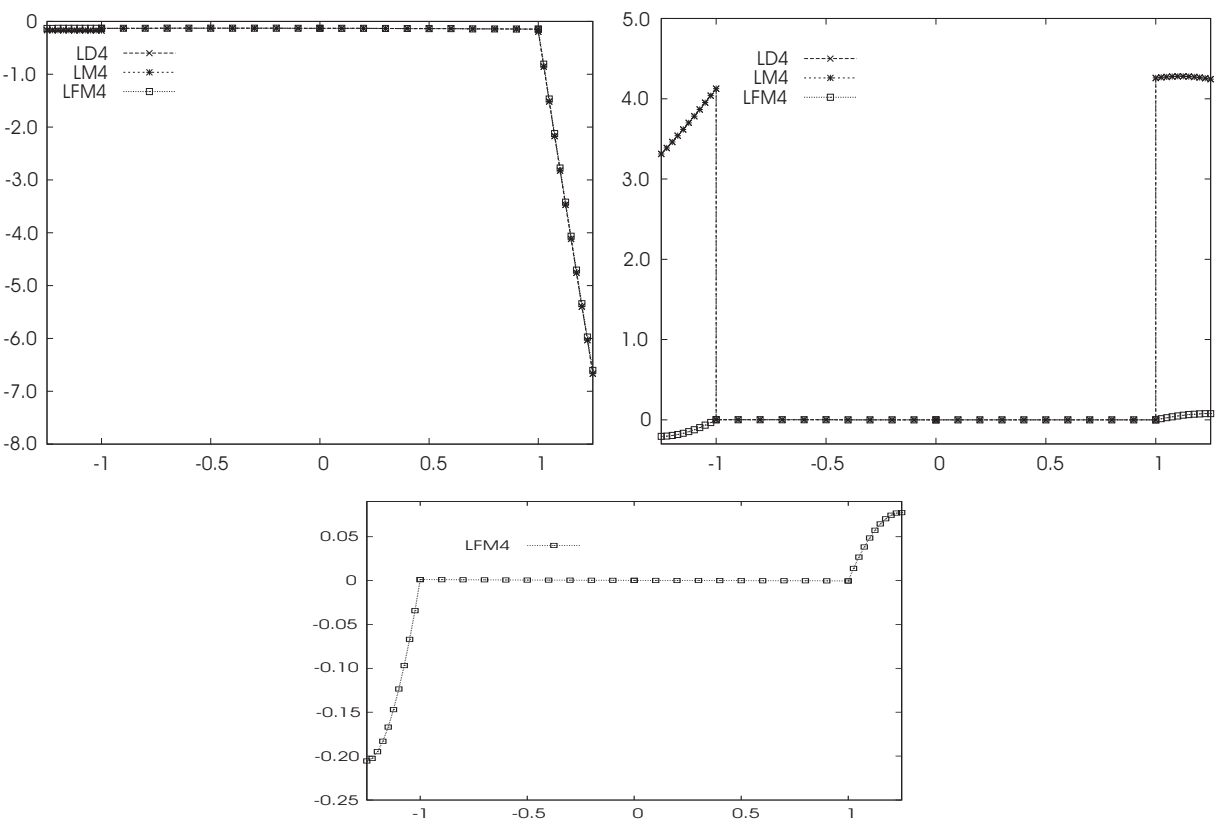

Figure 6. Proposed benchmark: plot of $\mathcal{D}_z 10^{10}$ versus z for multilayer piezoelectric shell, with $R_\beta/h = 10$. Top left, actuator case; top right, sensor case. The bottom figure plots the zoom of LFM4 results of sensor case.

R_β/h	2	4	10	100	R_β/h	2	4	10	100
		Φ $(z=0)$					Φ $(z=0)$		
LD4	0.4064	0.4829	0.5029	0.5009	LD4	0.0039	0.0157	0.0485	0.3414
LM1	0.4014	0.4824	0.5029	0.5009	LM1	0.0036	0.0154	0.0484	0.3415
LM4	0.4064	0.4829	0.5029	0.5009	LM4	0.0039	0.0157	0.0485	0.3414
LFM1	0.3805	0.4784	0.5041	0.5012	LFM1	0.0013	0.0133	0.0458	0.3287
LFM2	0.4059	0.4827	0.5029	0.5009	LFM2	0.0038	0.0156	0.0485	0.3414
LFM3	0.4065	0.4829	0.5029	0.5009	LFM3	0.0039	0.0157	0.0485	0.3414
LFM4	0.4064	0.4829	0.5029	0.5009	LFM4	0.0039	0.0156	0.0485	0.3414
		$\mathcal{D}_z 10^9$ $(z=h/2)$					$\mathcal{D}_z 10^{11}$ $(z=h/2)$		
LD4	−1.0754	−0.6666	−0.3322	−0.3494	LD4	9.8912	42.445	391.73	227910
LM1	−0.6686	−0.4157	−0.2172	−0.3373	LM1	5.1565	31.407	347.52	225160
LM4	−1.0754	−0.6666	−0.3322	−0.3494	LM4	9.8858	42.441	391.73	227910
LFM1	−1.0844	−0.6674	−0.3285	−0.3623	LFM1	1.1188	1.6464	1.9872	−1.6061
LFM2	−1.0639	−0.6600	−0.3268	−0.3622	LFM2	0.5401	0.6890	0.8068	−2.5408
LFM3	−1.0655	−0.6603	−0.3269	−0.3622	LFM3	0.6220	0.7813	0.9010	−2.4677
LFM4	−1.0654	−0.6603	−0.3269	−0.3622	LFM4	0.6092	0.7747	0.9001	−2.4676
		$W 10^{11}$ $(z=0)$					$W 10^9$ $(z=0)$		
LD4	−1.1542	−1.0208	−1.0048	2.4869	LD4	0.2633	0.9437	7.9334	4403.2
LM1	−1.2671	−1.0582	−1.0290	2.4730	LM1	0.2548	0.9386	7.9314	4404.3
LM4	−1.1542	−1.0208	−1.0048	2.4869	LM4	0.2633	0.9437	7.9334	4403.2
LFM1	−1.2320	−1.0342	−1.0112	2.4838	LFM1	0.2539	0.9377	7.9271	4403.0
LFM2	−1.1362	−1.0171	−1.0043	2.4869	LFM2	0.2623	0.9426	7.9307	4403.2
LFM3	−1.1560	−1.0209	−1.0048	2.4869	LFM3	0.2634	0.9438	7.9335	4403.2
LFM4	−1.1542	−1.0208	−1.0048	2.4869	LFM4	0.2633	0.9437	7.9334	4403.2
		σ_{zz} $(z=h/2)$					σ_{zz} $(z=-h/2)$		
LD4	0.1416	0.0902	0.0757	−0.1835	LD4	−2.2444	−6.0302	−52.912	−32549
LM1	−0.0062	0.0021	0.0023	0.0006	LM1	−1.1772	−1.0658	−0.8449	11.453
LM4	0.0000	0.0000	0.0000	0.0000	LM4	−1.0013	−1.0010	−1.0006	−1.0000
LFM1	0.0055	0.0074	0.0043	0.0008	LFM1	−1.1791	−1.0667	−0.8440	11.512
LFM2	0.0008	0.0000	0.0001	0.0000	LFM2	−0.9992	−1.0172	−1.0857	−1.7388
LFM3	0.0001	0.0000	0.0000	0.0000	LFM3	−0.9983	−1.0057	−1.0087	−1.0071
LFM4	0.0000	0.0000	0.0000	0.0000	LFM4	−1.0013	−1.0010	−1.0006	−0.9999

Table 7. Proposed benchmark: multilayer piezoelectric shell in the Varadan–Bhaskar geometry (Figure 4). Comparison of approaches. Left, actuator case; right, sensor case.

References

[Ballhause et al. 2004] D. Ballhause, M. D'Ottavio, B. Kröplin, and E. Carrera, "A unified formulation to assess multilayered theories for piezoelectric plates", *Comput. Struct.* **83**:15–16 (2004), 1217–1235.

[Carrera 1998] E. Carrera, "Evaluation of layer-wise mixed theories for laminated plates analysis", *AIAA J.* **36** (1998), 830–839.

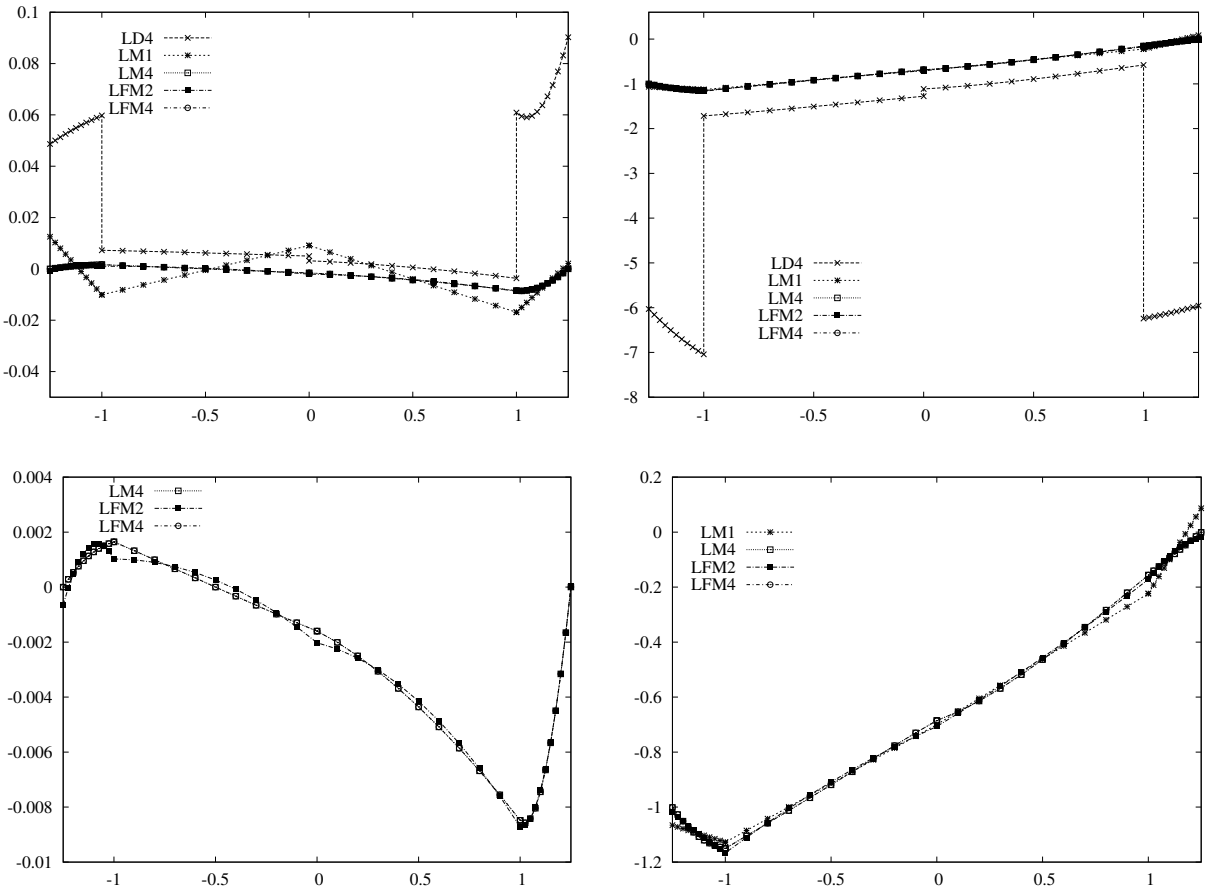

Figure 7. Proposed benchmark: plot of σ_{zz} versus z for multilayer piezoelectric shell, with $R_\beta/h = 4$. Left, actuator case; right, sensor case. The lower panes show details of the graphs. Mixed and full mixed theories are considered.

[Carrera 1999a] E. Carrera, "Multilayered shell theories accounting for layerwise mixed description, 1: governing equations", *AIAA J.* **37**:9 (1999), 1107–1116.

[Carrera 1999b] E. Carrera, "Multilayered shell theories accounting for layerwise mixed description, 2: numerical evaluations", *AIAA J.* **37**:9 (1999), 1117–1124.

[Carrera 2001] E. Carrera, "Developments, ideas and evaluations based upon the Reissner's Mixed Theorem in the modelling of multilayered plates and shells", *Appl. Mech. Rev.* **54**:4 (2001), 301–329.

[Carrera 2003] E. Carrera, "Theories and finite elements for multilayered plates and shells: a unified compact formulation with numerical assessment and benchmarking", *Arch. Comput. Methods Eng.* **10**:3 (2003), 215–296.

[Carrera and Boscolo 2006] E. Carrera and M. Boscolo, "Classical and mixed finite elements for static and dynamics analysis of piezoelectric plates", *Int. J. Numer. Methods Eng.* (2006). Published online 6 Nov 2006.

[Carrera and Brischetto 2007] E. Carrera and S. Brischetto, "Reissner mixed theorem applied to bending analysis of piezoelectric shells", *J. Intell. Mater. Syst. Struct.* (2007). In press.

[Carrera and Fagiano 2007] E. Carrera and C. Fagiano, "Full and partial extension of mixed finite elements for static analysis of piezoelectric plates", *J. Intell. Mater. Syst. Struct.* (2007). In press.

[Chen et al. 1996] C.-Q. Chen, Y.-P. Shen, and X.-M. Wang, "Exact solution of orthotropic cylindrical shell with piezoelectric layers under cylindrical bending", *Int. J. Solids Struct.* **33**:30 (1996), 4481–4494.

[Cho and Roh 2003] M. Cho and H. Y. Roh, "Development of geometrically exact new shell elements based on general curvilinear co-ordinates", *Int. J. Numer. Methods Eng.* **56**:1 (2003), 81–115.

[Chopra 2002] I. Chopra, "Review of state of art of smart structures and integrated systems", *AIAA J.* **40**:11 (2002), 2145–2187.

[Crawley 1994] E. F. Crawley, "Intelligent structures for aerospace: a technology overview and assessment", *AIAA J.* **32**:8 (1994), 1689–1699.

[D'Ottavio and Kröplin 2006] M. D'Ottavio and B. Kröplin, "An extension of Reissner mixed variational theorem to piezoelectric laminates", *Mech. Adv. Mater. Struct.* **13**:2 (2006), 139–150.

[D'Ottavio et al. 2006] M. D'Ottavio, D. Ballhause, B. Kröplin, and E. Carrera, "Closed-form solutions for the free vibration problem of multilayered piezoelectric shells", *Comput. Struct.* **84**:22–23 (2006), 1506–1518.

[Dumir et al. 1997] P. Dumir, G. Dube, and S. Kapuria, "Exact piezoelastic solution of simply-supported orthotropic circular cylindrical panel in cylindrical bending", *Int. J. Solids Struct.* **34**:6 (1997), 685–702.

[Garcia Lage et al. 2004] R. Garcia Lage, C. M. Mota Soares, C. A. Mota Soares, and J. N. Reddy, "Layerwise partial mixed finite element analysis of magneto-electro-elastic plates", *Comput. Struct.* **82**:17–19 (2004), 1293–1301.

[Heyliger 1997] P. Heyliger, "Exact solutions for simply suported laminated piezoelectric plates", *J. Appl. Mech.* (*ASME*) **64** (1997), 299–306.

[Heyliger et al. 1996] P. Heyliger, K. C. Pei, and D. Saravanos, "Layerwise mechanics and finite element model for laminated piezoelectric shells", *AIAA J.* **34**:11 (1996), 2353–2360.

[Ikeda 1996] T. Ikeda, *Fundamentals of piezoelectricity*, Corrected paperback ed., Oxford Science Publications, Oxford University Press, New York, 1996.

[Kögl and Bucalem 2005] M. Kögl and M. L. Bucalem, "Analysis of smart laminates using piezoelectric MITC plate and shell elements", *Comput. Struct.* **83**:15–16 (2005), 1153–1163.

[Lammering and Mesecke-Rischmann 2003] R. Lammering and S. Mesecke-Rischmann, "Multifield variational formulations and related finite elements for piezoelectric shells", *Smart Mater. Struct.* **12**:6 (2003), 904–913.

[Murakami 1986] H. Murakami, "Laminated composite plates theory with improved in-plane response", *J. Appl. Mech.* (*ASME*) **53** (1986), 661–666.

[Reddy 2004] J. N. Reddy, *Mechanics of laminated composite plates and shells: theory and analysis*, CRC Press, Boca Raton, FL, 2004.

[Ren 1987] J. G. Ren, "Exact solutions for laminated cylindrical shells in cylindrical bending", *Compos. Sci. Technol.* **29**:3 (1987), 169–187.

[Robaldo et al. 2006] A. Robaldo, E. Carrera, and A. Benjeddou, "A unified formulation for finite element analysis of piezoelectric adaptive plates", *Comput. Struct.* **84**:22–23 (2006), 1415–1505.

[Robbins and Chopra 2006] D. H. Robbins and I. Chopra, "The effect of laminated kinematic assumptions on the global response of actuated plates", *J. Intell. Mater. Syst. Struct.* **17**:4 (2006), 273–299.

[Rogacheva 1994] N. L. Rogacheva, *The theory of piezoelectric shells and plates*, CRC Press, Boca Raton, FL, 1994.

[Saravanos and Heyliger 1999] D. A. Saravanos and P. R. Heyliger, "Mechanics and computational models for laminated piezoelectric beams, plates, and shells", *Appl. Mech. Rev.* **52**:10 (1999), 305–320.

[Shakeri et al. 2006] M. Shakeri, M. Eslami, and A. Daneshmehr, "Dynamic analysis of thick laminated shell panel with piezoelectric layer based on three dimensional elasticity solution", *Comput. Struct.* **84**:22–23 (2006), 1519–1526.

[Varadan and Bhaskar 1991] T. K. Varadan and K. Bhaskar, "Bending of laminated orthotropic cylindrical shells: an elasticity approach", *Compos. Struct.* **17**:2 (1991), 141–156.

[Wang et al. 2005] H. M. Wang, H. J. Ding, and Y. M. Chen, "Dynamic solution of a multilayered orthotropic piezoelectric hollow cylinder for axisymmetric plane strain problems", *Int. J. Solids Struct.* **42**:1 (2005), 85–102.

Received 24 Jul 2006. Accepted 9 Oct 2006.

ERASMO CARRERA: erasmo.carrera@polito.it
Dept. of Aeronautics and Aerospace Engineering, Politecnico di Torino, Corso Duca degli Abruzzi, 24, 10129 Torino, Italy

SALVATORE BRISCHETTO: salvatore.brischetto@polito.it
Dept. of Aeronautics and Aerospace Engineering, Politecnico di Torino, Corso Duca degli Abruzzi, 24, 10129 Torino, Italy